Accepted Manuscript

Structure-based development of an osteoprotegerin-like glycopeptide that blocks RANKL/RANK interactions and reduces ovariectomy-induced bone loss in mice

Chao Liu, Xiao Chen, Xin Zhi, Weizong Weng, Quan Li, Xiang Li, Yan Zou, Jiacan Su, Hong-Gang Hu

PII: S0223-5234(18)30022-9

DOI: 10.1016/j.ejmech.2018.01.022

Reference: EJMECH 10099

To appear in: *European Journal of Medicinal Chemistry*

Received Date: 1 November 2017

Revised Date: 3 January 2018

Accepted Date: 8 January 2018

Please cite this article as: C. Liu, X. Chen, X. Zhi, W. Weng, Q. Li, X. Li, Y. Zou, J. Su, H.-G. Hu, Structure-based development of an osteoprotegerin-like glycopeptide that blocks RANKL/RANK interactions and reduces ovariectomy-induced bone loss in mice, *European Journal of Medicinal Chemistry* (2018), doi: 10.1016/j.ejmech.2018.01.022.

Graph Abstract

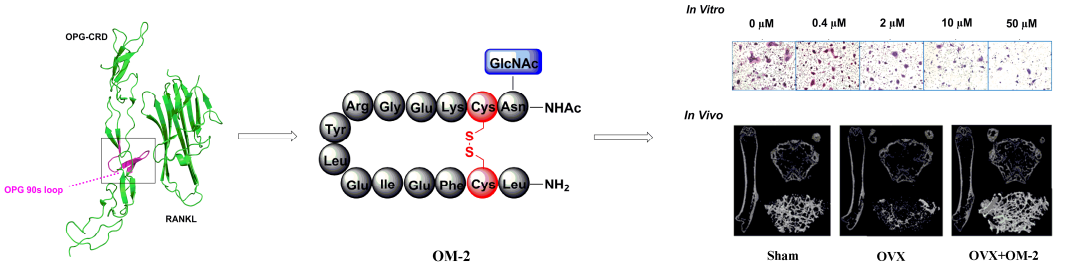

Crystal structure-based develpment of osteoprotegerin-like peptide mimics

Chemical structure optimization and biological screen to obtain glycopeptide OM-2

In Vitro dose-dependent assay and *In Vivo* biological test to comfirm the inhibitory activity of OM-2

Structure-based Development of an Osteoprotegerin-like Glycopeptide That Blocks RANKL/RANK Interactions and Reduces Ovariectomy-induced Bone Loss in Mice

Chao Liu [1], Xiao Chen [2], Xin Zhi [3], Weizong Weng [2], Quan Li [2], Xiang Li[1], Yan Zou[1]*, Jiacan Su [2]*, Hong-Gang Hu[1]*

1. Department of Organic Chemistry, College of Pharmacy, Second Military Medical University, Shanghai 200433, China

2. Department of Orthopedics Trauma, Shanghai Changhai Hospital, Second Military Medical University, Yangpu District, Shanghai 200433, China

3. Graduate Management Unit, Shanghai Changhai Hospital, Second Military Medical University, Yangpu District, Shanghai 200433, China

Chao Liu and Xiao Chen contributed equally to this work.

*Corresponding to Prof. Yan Zou, Email: zouyan@smmu.edu.cn; Prof. Jiacan Su, Email:drsujiacan@163.com; Prof. Hong-Gang Hu, Email: hhu66@smmu.edu.cn.

Abstract

Osteoporosis is a metabolic bone disease characterized by low bone mass and micro-architectural deterioration of bone, for which the underlying mechanism is an imbalance between bone resorption and bone remodeling. The protein-protein interactions between receptor activator of nuclear factor-κB ligand (RANKL), RANK (its receptor), and osteoprotegerin (OPG), are known to mediate the development and activation of osteoclasts in bone remodeling, and are regarded as a pivotal therapeutic target for the treatment of osteoporosis. Herein, we disclose the successful development of a novel glycopeptide (OM-2), the structure of which is based on the key interacting sites of the reported RANKL and OPG crystal structure. OM-2 exhibited potent binding affinity with RANKL and resistance to degradation by protease enzymes. It also blocked RANKL/RANK interactions, and inhibited osteoclastogenesis *in vitro*. *In vivo* studies confirmed that OM-2 could effectively reduce bone loss and inhibit osteoclast activation in ovariectomized (OVX) mice at a dosage of 20.0 mg/kg/day. Accordingly, OM-2 is suggested as a therapeutic candidate for postmenopausal osteoporosis (PMOP) and osteoclastogenesis-related diseases like rheumatoid arthritis (RA). More importantly, its identification validates our structure-based strategy for the development of drugs that target the RANKL/RANK/OPG system.

Keywords: Osteoprotegerin; Mimics; Glycopeptide; RANKL; Osteoclastogenesis

1. Introduction

Diseases caused by the excessive activation of osteoclasts such as postmenopausal osteoporosis (POMP) and rheumatoid arthritis constitute a worldwide threat to public health [1,2]. Osteoporosis is characterized by low bone mineral density (BMD) and poor bone quality, leading to high risk of fragility fractures [3]. Worldwide, more than 8.9 million people have experienced osteoporosis-stimulated fractures over the past decade, and the World Health Organization (WHO) has identified osteoporosis as a major public health concern [4].

The use of therapeutic agents that inhibit osteoclastogenesis and restore the balance between bone resorption and formation is an important strategy for the treatment of osteoporosis [5]. Bisphosphonates are widely used to rectify osteoclast-induced bone resorption in osteoporosis, but their use is severely limited due to their poor bioavailability and gastrointestinal tolerability, renal toxicity, and tendency to cause osteonecrosis of the jaw [6-9]. Possible alternative anti-resorption drugs include selective estrogen receptor modulators (SERM) and strontium ranelate, but the side-effects of these include thromboembolic disease, drug rash with eosinophilia systemic syndrome, and abdominal discomfort [6,7]. Bone-anabolic drugs are limited to teriparatide, an *N*-terminal fragment of parathyroid hormone (PTH 1-34), which stimulates bone formation by regulating osteoblast numbers and activity. Side-effects of this drug include back pain, nausea, leg cramps, dizziness and osteosarcoma, which limit the duration of therapy [8,9]. Accordingly, novel treatments for osteoporosis are urgently needed [10,11].

The RANKL/RANK/OPG system plays a vital role in osteoclastogenesis [12-18]. RANK is expressed on osteoclast precursors and can be activated by its native ligand RANKL, which leads to osteoclast differentiation, maturation, and bone resorption [12,13,17,19-24]. Meanwhile, by acting as a soluble decoy receptor to RANKL, OPG competes with RANK for RANKL binding to inhibit osteoclastogenesis [12,18,19,25]. Various osteolytic bone diseases such as primary osteoporosis, rheumatoid arthritis and osteolytic bone metastases result from an imbalance between osteogenesis and osteoclastogenesis [26-28], and over-activated osteoclasts play a leading role in disease pathogenesis [17,18,29,30]. Accordingly, blocking the RANKL/RANK interaction to inhibit osteoclastogenesis is a promising therapeutic strategy [31,32].

RANK-Fc, Fc-osteoprotegerin and anti-RANKL antibodies have been previously used to block the RANKL/RANK interaction [33,34]. Denosumab is a RANKL monoclonal antibody inhibitor and has been used for osteoporosis patients at a high risk of fracture, bone loss due to certain medications, and bone metastases [35-39]. However, it is very expensive, and

causes hypocalcemia side effect [40,41]. Moreover, low stability, poor bioavailability, high cost and difficulties in administration were the major disadvantages hindered the appication of large macromolecules for therapeutic intervention [42]. Therefore, small peptides or peptidomimetic-based treatments are another option, and their unique chemical properties, proper molecular weight, improved biological activity, low toxicity, and immunogenicity could overcome these drawbacks [43,44]. Also, the specific nature of their target, weak drug-drug interactions, and reduced propensity to accumulate in tissue, reduce the risk of complications associated with their use [43]. In previous study, disulfide bond bearing peptides from RANK/RANKL interaction such as WP9QY and L3-3 were developed and their inhibitory activity was confirmed *in vivo* [45,46]. Effective OPG-like peptide mimics were limited to disulfide bond peptide OP3-4 and linear peptide YR-11. They have been shown to inhibit RANKL-induced osteoclastogenesis both *in vitro* and *in vivo*, prevent osteolytic bone disease in myeloma and down regulate inflammatory cytokines [42,47,48]. Nevertheless, these designs were only based on the putative contacts derived from the co-crystal structures of TNF-β·TNFR1 or deduced OPG binding sites to RANKL, with no authentic crystal structure-based evidence.

In 2012, the structure of human RANKL ectodomain complexed with the *N*-terminal of human OPG cysteine-rich TNFR homologous domains (OPG-CRD) was clarified, providing precise molecular details of the RANKL/OPG interactions, and a structural basis for the rational design of OPG-like peptides or peptidomimetics for the purpose of interrupting ligand-receptor interaction [49]. Herein, we disclose the development of several OPG-like peptides or peptidomimetics, guided by the crystal-structure of RANKL/OPG complex (PDB: 3URF). RANKL-induced osteoclastogenesis inhibition was verified *in vitro*, and OM-2 was identified as the most potent inhibitor. The circular dichroism (CD) spectroscopy, binding affinity, protease resistance and effect on downstream signaling pathways of OM-2 were then investigated, and its *in vivo* effects were evaluated in ovariectomized mice.

2. Results

2.1. Structural-based design and synthesis of OPG-like mimics

The binding interface of RANKL/OPG-CRD presents two binding sites (**Figure S1A**) [49]. The first, binding site I, consists of small and separate interactions, is located on the OPG "50s loop" (His^{47}-Leu^{65}) of the CRD-2 domain, and extends along and parallel to the groove of RANKL. Binding site II, located at the OPG "90s loop" (Arg^{90}-Leu^{98}) of the CRD-3 domain, is deeply within the groove, and flanked by AA' and CD loops of RANKL. Binding site II uses the Glu^{95} of the OPG "90s loop" to form a hydrophilic interaction network with RANKL residues Arg^{223}, Tyr^{241} and Lys^{257}, and is more important than binding site I in RANKL/OPG-CRD binding. Furthermore, this location is also the major binding determinant of RANKL/RANK interaction. Accordingly, peptides or peptidomimetics whose sequences are derived from the OPG "90s loop" are hypothesized to inhibit protein-protein interactions (PPIs). Moreover, multiple disulfide bridges are separated on the OPG CRD-3 sequence, and the disulfide bonds between Cys^{86} and Cys^{97} are distributed around the OPG "90s loop" sequence. This fragment is vital for its interaction with the AA' and CD loop of RANKL.

Initially, we designed disulfide peptide **OM-1** (**Figure 1**) based on the Cys^{86}–Leu^{98} fragment, to obtain the shortest peptide with definite secondary structure. **OM-1** was synthesized *via* a solid phase coupling/solution phase cyclization strategy. The on-resin peptide **1** was cleavaged from the solid support to obtain the free peptide **2**. The following oxidative folding [6 M Gn·HCl/100 mM NaH_2PO_4 PBS buffer (pH=7.4) containing 10 % DMSO] of **2** provided the disulfide peptide **OM-1** in an overall yield of 40.0 % (**Scheme 2**). However, given the propensity of disulfide bond-bearing peptides to degrade in the physiological environment through reduction, polymerization or enzymatic cleavage of the disulfide bond [50-52], we next sought to optimize OM-1 by chemical means, such as by glycosylation or by stabilization of the disulfide-bond.

It was found that multiple *N*-linked *N*-acetyl-glucosamine glycosylation sites are present on the OPG backbone [48,49]. Although the functions of these glycosylation sites remains

unclear, glycosylation has been demonstrated to exert a multifaceted influence on the chemical properties and function of peptides, including improved hydrophilicity and bioavailability, better conformation restriction and maintenance, increased protease resistance, and weaker immunogenicity [53]. Furthermore, chondroitin sulfate combined with glucosamine sulfate could increase the expression ratio of OPG/RANKL, indicating a potential regulative function in the RANK/RANKL/OPG system of carbohydrates [54]. However, it was suggested that an inappropriate spatial location of the carbohydrate block might impart significant structural and conformational changes upon the peptide, and perturb the interactions between the peptide and target protein [53]. In order to design a reasonable glycopeptide mimic, we undertook a hypothetical geometry comparison and molecular docking study to investigate the proper location for the carbohydrate block. The results suggested that, compared with the non-glycosylated form, arrangement of the carbohydrate group at the tail of peptide back bone has little impact on the peptide secondary structure and didn't disturb the mutual binding mode. As shown in **Figure S1B**, the locations of all the amino acid side chains matched the non-glycosylated form. Furthermore, upon binding to the active sites of RANKL, the Ile^{94} and Leu^{96} residues were found to form hydrophobic and *van der Waals* interactions with the surrounding hydrophobic residues of RANKL. More importantly, Glu^{95} was found to be the key interaction residue, forming multiple *H*-bonds with Lys^{257} and Tyr^{241} of RANKL (**Figure S1C**). It was with these observations in mind, glycopeptide mimic **OM-2** (**Figure 1**) was designed.

The synthesis of **OM-2** was based on the key glycoamino acid building block Fmoc-Asn[GlcNAc(Ac_3)]-OH (**5**). *N*-acetyl-β-D-glucosamine was selected as the starting material, and after acetylation followed by reaction with sodium azide catalyzed by the phase transfer catalyst tetrabutylammonium iodide, compound **3** was obtained in an 82.4 % yield. Reduction of the azide group followed by coupling with Fmoc-Asp-O^{t}Bu through 1-hydroxybenzotriazole (HOBt)/*N*,*N*'-diisopropylcarbodiimide (DIC) led to the protected glycoamino acid building block **4**, which underwent ^{t}Bu deprotection using a TFA/DCM

solution to give the target compound **5** in good yield (95.0 %, **Scheme 1A**). Compound **5** was readily incorporated into the peptide backbone through standard Fmoc SPPS using O-(7-azabenzotriazol-1-yl)-*N*,*N*,*N'*,*N'*-tetramethyluronium hexafluorophosphate (HATU) as the coupling reagent, to obtain on-resin peptide **6**. The following on-resin deprotection of the acetyl protection group utilizing hydrazine hydrate gave the on-resin intermediate **7**. After acidic cleavage, global deprotection and oxidative folding, **OM-2** was obtained in a yield of 25.2 % (**Scheme 2**).

We considered two alternatives to the disulfide bond of peptide OM-1. Firstly, diselenide peptides have been shown to impart greater biological activity than their disulfide counterparts, perhaps due to a different bond connectivity and/or conformational structure resulting from the diselenide substitution, which is more metabolically stable than the disulfide linkage [55,56]. Accordingly, peptide **OM-3** (**Figure 1**) containing a diselenide bridge was synthesized, with view to improving the biological activity and pharmacokinetic properties of peptide OM-1. By incorporating (S)-2-((((9H-fluoren-9-yl)methoxy)carbonyl) amino)-3-((4-ethoxybenzyl)selanyl) propanoic acid [Fmoc-Sec(Mob)-OH] into standard SPPS, we assembled the protected on-resin peptide **8**. After cleavage from the solid support, the Mob protected peptide **9** was treated with TFA/DMSO solution (1:1, *v/v*) to complete the final deprotection and folding step, giving the diselenide peptidomimetic **OM-3** in 27.4 % yield (**Scheme 2**).

Secondly, in view of its chemical orthogonality and its imperviousness to isomerases and proteases, the triazole bridge was also selected to replace the disulfide-bond. Thus, the 1,4-disubstituted 1,2,3-triazole bridge mimic **OM-4** (**Figure 1**) was obtained using a diaminodiacid-based synthetic strategy, according to our previous report [57]. Briefly, Boc-Dap-OH was transformed into 3-azido-*N*-Boc-L-alanine (**10**) *via* a Cu(II)-catalyzed diazo transfer reaction. Then, the tert-butoxycarbonyl (Boc) group of **10** was easily cleaved by trifluoroacetic acid, and the free amino acid was further protected with allyloxycarbonyl (Alloc) and allyl groups to afford **11**. Installation of the tert-butyl (^{t}Bu) protective group

followed by capping of 9*H*-fluoren-9-ylmethoxy)carbonyl (Fmoc) group on 2-propargyl-L-glycine (H-Pra-OH) provided Fmoc-Pra-O^{t}Bu (**12**). Compound **13** could be obtained through copper(I)-catalyzed azide-alkyne cycloaddition (CuAAC) reaction between **11** and **12** directly in a high chemical yield. Finally, the diaminodiacid building block **14** was prepared from **13** by removing the ^{t}Bu protection group using trifluoroacetic acid (**Scheme 1B**). Next, **14** was successfully attached to resin through standard Fmoc SPPS using HATU as the coupling reagent, to obtain on-resin peptide **15**. After cleavage of the protective allyl, Alloc and Fmoc groups *via* $[Pd(PPh_3)_4]/PhSiH_3$ and 20 % piperidine/DMF solution, macrocyclization was successfully accomplished with (7-azabenzotriazol-1-yloxy)tripyrrolidinophosphonium hexafluorophosphate (PyAOP), N-methylmorpholine (NMM) and 1-hydroxy-7-azabenzotriazole (HOAt) as lactamization reagents, to achieve cyclic peptide **16**. Finally, one step global deprotection and cleavage with the TFA cocktail delivered **OM-4** in a yield of 32.1 % (**Scheme 2**). To the best of our knowledge, this is the first time that glycopeptide, disulfide, diselenide, and triazole-bridged derivatives of the same peptide have been systematically synthesized and tested in a RANK/RANKL/OPG system study.

2.2. Biological test *in vitro* and cytotoxicity study

OPG mimics were evaluated *via* tartrate-resistant acid phosphatase (TRAP) staining to screen for biological activity against RANKL-induced osteoclast differentiation on bone marrow mononuclear cells (BMMCs) [46]. Each mimic (30.0 μM) was co-cultured with RANKL and macrophage colony-stimulating factor (M-CSF) in BMMCs, and were found to exhibit inhibitory effects on the TRAP activity ranging from 24.35 % to 59.20 % on the 3rd day of induction (**Figure 2A**). OM-3 and OM-4, with 40.65 % and 42.15 % respectively, were more potent inhibitors than OM-1 (24.35 %). Glycopeptide OM-2 exhibited greater inhibitory potency than the positive control peptide OP3-4, a previously reported OPG-like peptide mimic (58.20 % for OM-2; 55.57 % for OP3-4). Further tests at different concentrations of OM-2 and OP3-4 were then carried out by TRAP staining. OM-2 was found to reduce the number of TRAP-positive multinucleated cells in a dose-dependent manner

(**Figure 2B and Table S1**). The IC_{50} was 28.51 μM for OM-2 and 25.27 μM for OP3-4, implying that OM-2, an OPG-like glycopeptide mimic, could effectively suppress osteoclastogenesis *in vitro*. Subsequently, cell counting kit-8 (CCK-8) analysis was performed on BMMCs to test the potential toxicity. The results showed that even at 100.0μM treatments, these peptide mimics did not exhibit obvious cytotoxic effects, indicating the inhibitory activities were not due to their cytotoxicity (**Figure S6**).

2.3. CD spectroscopy of peptides and kinetic binding ability of OM-2

The secondary structures of the peptide mimics were analyzed by CD spectroscopy (**Figure 3A**). All the peptides showed a broad negative peak around 215 nm, characteristic of a *β*-sheet structure. This result suggested that the carbohydrate group on OM-2 has little impact on the secondary structure compared to OM-1. The binding affinity of OM-2 to RANKL was next investigated *via* surface plasmon resonance (SPR). OM-2 was found to bind to RANKL in a dose-dependent manner. The apparent association (k_{on}) and disassociation constants (k_{off}) of OM-2 were estimated to be 608.7 $M^{-1}s^{-1}$ and 0.0027 s^{-1} respectively, and the relative binding affinity (K_d) to RANKL was 4.54 μM (**Figure 3B**); weaker than the affinity of RANKL to RANK (RANKL to RANK K_d=13.9 nM) or OPG (RANKL to OPG K_d=17.6 nM), but comparable than that between RANKL and the positive OP3-4 peptide (**Figure S7**, OP3-4 to RANKL K_d=2.75 μM), suggesting the complex between RANKL and OM-2 to be relatively stable. The improved binding ability compared with OM-1 (**Figure 3C**, OM-1 to RANKL K_d=30.91 μM), is speculated to be attributable to the presence of carbohydrate structure into peptide backbone. Although the mechanism for binding between each peptide and RANKL is not clear without the crystal-structure of the OM-2/RANKL complex, the data obtained definitively establishes that glycopeptides OM-2 possess superior chemical and biological properties for the purposes of RANKL inhibition than normal peptides.

2.4. Inhibition of NF-κB by OM-2

The differentiation of osteoclast precursors into mature osteoclastsis associated with RANKL-stimulated NF-κB activation [23]. The activation of the NF-κB signal pathway is

indicated by the procedural activation of its inhibitory subunit IκB, including phosphorylation, ubiquitination, degradation, and nuclear localization signaling exposure [58]. To evaluate the effects of OM-2 on RANKL induced NF-κB activation, a western blotting study was carried out. The results showed that OM-2 could significantly inhibit RANKL-stimulated NF-κB activation as indicated by the lack of IκB phosphorylation (**Figure 3D**). This study shows that OM-2 effectively inhibits osteoclast formation, in part by interruption of the RANK/RANKL protein-protein interaction and suppression of the NF-κB signaling pathway. .

2.5. α-chymotrypsin resistance of OM-2

α-chymotrypsin is a protease that preferentially cleaves peptide amide bonds where the side-chain of the amino acid *N*-terminal to the scissile amide bond is a large, hydrophobic amino acid such as Trp, Phe and Leu, and is used for peptide protease stability studies [59]. OM-1 and OM-2 were subjected to the α-chymotrypsin mediated degradation test and monitored by HPLC. Even after 8 hours' protease exposure, more than 60.70 % OM-2 remained intact with a superior protease resistance compared with OM-1 (38.47 %), suggesting greater protease stability over normal peptides (**Figure 3E**). The improved *in vitro* inhibitory activity could partly result from the greater protease resistance [53].

2.6. Effects of OM-2 in OVX mice

The effects of OM-2 on ovariectomy-induced bone loss in mice were investigated. Six weeks after the surgery, OVX mice treated with normal saline exhibited a significant loss of trabecular bone in the distal femur. Intraperitoneal injection of OM-2 (20.0 mg/kg/day) in OVX mice markedly inhibited trabecular bone loss compared with OVX mice, as shown by hematoxylin and eosin (H&E) staining (**Figure 4A**). The number of osteoclasts was examined by TRAP staining. OM-2 significantly decreased the proportion of TRAP positive cells in femur bone (**Figure 4B**). These results were corroborated by micro-computed tomography (Micro CT). **Figure 4C** and **Figure 4D** depict the two-dimensional and three-dimensional structures of the bone, as measured by trabecular bone volume expressed per unit total volume (BV/TV), trabecular bone surface area expressed per unit total volume (BS/TV),

trabecular number (Tb. N) and BMD. Compared with the OVX group, OVX+OM-2 group displayed decreased serum interleukin 6 (IL-6), tumor necrosis factor alpha (TNF-α), serum C-terminal telopeptide of type I collagen (CTX-1) and tartrate-resistant acid phosphatase 5B (TRAcp5B) ($P< 0.05$) levels, suggesting that OM-2 inhibited bone loss in OVX mice by inhibition of osteoclastogenesis (**Figure 4E**).

3. Discussion

Four OPG-like peptides OM-1, OM-2, OM-3 and OM-4 or peptidomimetics have been designed based on the crystal structure of human RANKL/OPG-CRD complex and synthesized by SPPS, in order to test their ability to perturb RANK receptor signaling. *In vitro* studies showed that glycopeptide OM-2 was the most potent inhibitor of RANKL-induced osteoclastogenesis of all the peptides tested. It was able to effectively inhibit RANKL-mediated NF-κB signaling pathway in BMMCs and displayed improved binding affinity and superior protease resistance compared to OM-1. *In vivo* studies showed that OM-2 reduced OVX induced bone loss and osteoclast formation.

The RANKL/RANK/OPG axis is well known to regulate osteoclast differentiation and play a vital role in bone remodeling. Furthermore, RANKL is involved in various osteolytic pathogenesis processes such as primary osteoporosis, rheumatoid arthritis, bone metastases, *etc.*, and protein therapeutics such as RANK-Fc, Fc-osteoprotegerin and RANKL monoclonal antibodies that block RANKL activity are proven treatments for these diseases [33-39].

Denosumab was approved in 2010 for the treatment of postmenopausal women with osteoporosis at high risk of fracture. Small peptides derived from either RANK or OPG were also demonstrated to inhibit osteoclastogenesis both *in vitro* and *in vivo* [42,45-48]. However, prior to 2012, when the crystal structure of human RANKL/OPG-CRD complex was first revealed [49], there was no structural basis to inform OPG-like design. The crystal structure study suggests that RANKL employs distinct binding modes to engage RANK and the OPG receptor, and OPG binds to RANKL with a nearly 500-fold higher affinity and 150 times

greater inhibitory activity on RANKL-stimulated osteoclastogenesis than RANK [60]. Hence, we hypothesized that peptides derived from the key interacting site of OPG with RANKL would be more effective at disrupting RANKL/RANK interactions than from RANK. Accordingly, we designed and synthesized a disulfide peptide based on the OPG "90s loop" sequence, regarded as the critical binding site for OPG/RANKL interactions [49], to obtain the shortest fragment which could simulate its secondary structure. Thereafter, we carried out an *in vitro* osteoclastogenesis inhibitory study. BMMCs were isolated, and induced with RANKL (300.0 ng/mL) and M-CSF (30.0 ng/mL). Peptide OM-1 exhibited only weak inhibitory activity, possibly due to the susceptibility of disulfide bond present in its structure. To overcome this problem, we strategically modified the peptide structure. Many natural macrocyclic peptide antibiotics and physiologically active proteins are glycosylated, indicating the critical role of carbohydrates in sustaining physiological functions [61,62]. Additionally, glycosylation can improve chemical properties of peptides such as hydrophilicity, oral bioavailability, protease resistance, and conformation stability [53]. Also, the diselenide bridge is a well-known disulfide bond replacement strategy, widely used in peptide and protein folding studies, to provide greater conformation stability without adversely affecting biological activities [55,56]. Finally, the triazole bridge has been extensively investigated in peptide chemistry too, for the purpose of mimicking and adding rigidity to the amide backbone, and as a linking group in carbohydrate chemistry and vaccine preparation [63-66]. More importantly, triazole substitution has already been used as an effective replacement for the disulfide-bond [67,68]. Accordingly, three potential candidate peptides OM-2 (bearing a disulfide bond), OM-3 (bearing a diselenide bond) and OM-4 (bearing a triazole bridge) were synthesized and tested. Of these, OM-2 was found to exhibit the strongest inhibitory activity, as measured in a TRAP assay at 30.0 μM concentration, comparable to positive control OP3-4. Further studies found the IC_{50} of OM-2 and OP3-4 to be equal. Computational docking results suggested that the glycosylation did not affect the secondary structure of the peptide, and CD spectroscopy study confirmed our incorporation of

a carbohydrate block on OM-2 did not have a deleterious effect on its β-sheet structure. Furthermore, we believe that the Glu^{95} of OM-2 was essential for good biological activity, due to the formation of hydrogen bonding network with active sites of RANKL.

Next, OM-2 was subjected to protease resistance and SPR experiments. The data suggested OM-2 to have greater protease stability and stronger binding ability to RANKL compared with OM-1 (its non-glycosylated form), a possible explanation for its improved activity. An immunoblotting study found that both OM-2 and OP3-4 significantly suppressed the RANKL-induced NF-κB signaling pathway, as indicated by a reduction in IκB phosphorylation.

In vivo, an OVX mice model was used to observe the effects of OM-2 on OVX induced bone loss. We found that OM-2 significantly reduced bone loss in OVX mice, by H&E staining of the distal femur, and Micro CT analysis. For TRAP staining, OM-2 was found to significantly reduce the number of activated osteoclasts around the trabecula. The serum level of the bone resorption markers TRAcp5B and CTX-1 were also significantly reduced. In a previous study, inflammation was found to play an important role in osteoclast differentiation [69]. Therefore, the serum levels of TNF-α and IL-6 also imply that OM-2 significantly decreased the osteoclastogenesis *in vivo*. More importantly, *in vivo* experiments suggested that OM-2 could impart bone protection when administered *via* intraperitoneal injection [70], which is preferable to the intravenous mode of administration required by OP3-4.

In conclusion, the novel glycopeptide OM-2, the design of which was informed by the crystal structure of the RANKL/OPG complex, has been synthesized and found to inhibit osteoclastogenesis *in vitro*, with an IC_{50} of 28.51 μM, and reduce bone loss in OVX mice, at a dosage of 20.0 mg/kg/day. This study establishes OM-2 as a promising lead for the development of novel therapeutics for PMOP, as well as a variety of diseases caused by the over-expression of RANKL, such as rheumatoid arthritis, periodontal diseases and bone metastasis. Also, it constitutes a useful chemical tool for furthering our understanding of the molecular mechanisms and biological functions of the RANK/RANKL/OPG system. Further

optimization of OM-2 is ongoing in our laboratory, and the results will be disclosed in due course.

4. Experimental protocols

4.1. Materials

All chemical reagents were purchased from Acros, Sigma-Aldrich, Alfa Aesar, Adamas and InnoChem. Amino acids were obtained from GL Biochem Shanghai Co. Ltd; and all solvents were from Sinopharm Chemical Reagent Co. Ltd. Dichloromethane (DCM) and *N*,*N*-Dimethylformamide (DMF) were distilled over calcium hydride (CaH_2) under an argon atmosphere, and stored in flask containing 4 Å molecular sieves. All reactions vessels were oven-dried before use. Reactions were monitored by thin-layer chromatography (TLC) and visualized by UV (254 nm), ninhydrin and/or phosphomolybdic acid. Recombinant sRANKL, RANK and M-CSF were purchased from Sigma.

4.2. HPLC, Mass spectrometry and NMR

Peptides were analyzed and purified by reverse phase HPLC. A C18 analytic column (Shimadzu Shim-pack VP-ODS, 4.6×250 mm, 5 μm particle size, flow rate 1 mL/min) was used for analytical RP-HPLC, and a C18 column (Shimadzu Shim-pack PRC-ODS, 50×250 mm, 15 μm particle size, flow rate 13 mL/min) was used for semi-preparative RP-HPLC. The solvent systems were buffer A (0.1% TFA in CH_3CN) and buffer B (0.1% TFA in water). Data was recorded and analyzed using the software system LC Solution. High resolution mass spectra were measured on a Waters Xevo G2 QTOF mass spectrometer. ESI-MS was measured with a Bruker Esquire 3000 Plus Ion Trap mass spectrometer. ^{1}H-NMR and ^{13}C-NMR spectra were recorded on a Bruker Avance 300 MHz instrument. Chemical shifts (δ) are reported relative to TMS (0 ppm) for ^{1}H-NMR and ^{13}C-NMR spectra. Coupling constants (J) were given in Hertz (Hz); and the splitting patterns are abbreviated as follows: singlet (s); broad singlet (s, br); doublet (d); doublet of doublet (dd); triplet (t); quartet (q); multiplet (m).

4.3. Chemistry

*4.3.1. (2R,3S,4R,5R,6R)-5-acetamido-2-(acetoxymethyl)-6-azidotetrahydro-2H-pyran-3,4-diyldiacetate (**3**)*

To *N*-acetyl-*β*-D-glucosamine (10.00 g, 45.24 mmol) was added acetyl chloride (30.00 mL) dropwise over 15 min at 0 ºC. The reaction mixture was stirred vigorously at room temperature for 4 days. This mixture was diluted with DCM (100.00 mL) and saturated $NaHCO_3$ (100.00 mL) aqueous solution. The organic phase was separated, washed with saturated $NaHCO_3$ and brine (3×100.00 mL), dried over Na_2SO_4 and concentrated, and used without further purification. A mixture of commercially available NaN_3 (8.82 g, 135.70 mmol) and tetrabutylammonium iodide (16.68 g, 45.23 mmol) in DCM/water (1:1, 200.00 mL) was stirred for 2 hours at room temperature. The organic layer was separated, washed with brine (3×100.00 mL), dried over Na_2SO_4, concentrated and purified by column chromatography (6:1-2:1, petro ether/EtOAc) to give 3 as a white powder (13.80 g, 82.4 %, 2 steps). **^{1}H-NMR (300 MHz, $CDCl_3$):** δ 5.72 (d, *J*= 3.0 Hz, 1H), 5.25-5.22 (m, 1H), 5.10-5.07 (m, 1H), 4.75 (d, *J*= 3.0 Hz, 1H), 4.27-4.24 (m, 1H), 4.17-4.14 (m, 1H), 2.09 (s, 3H), 2.03 (s, 3H), 2.02 (s, 3H), 1.97 (s, 3H). **^{13}C-NMR (300 MHz, $CDCl_3$):** δ 172.40, 172.08, 171.84, 170.67, 89.83, 75.42, 73.57, 69.48, 63.27, 55.61, 24.64, 22.12, 22.03, 21.98. **ESI-MS m/z** calcd for $C_{14}H_{20}N_4O_8$ 372.13; found $[M+H]^+$ 373.29.

*4.3.2. (2R,3S,4R,5R,6R)-6-(3-((((9H-fluoren-9-yl)methoxy)carbonyl)amino)-4-(tert-butoxy)-4-oxobutanamido)-5-acetamido-2-(acetoxymethyl)tetrahydro-2H-pyran-3,4-diyl diacetate (**4**)*

To a solution of 3 (10.00 g, 26.88 mmol) in MeOH (200.00 mL) was added Pd/C catalyst (1.00 g). Then the mixture was stirred overnight at room temperature under hydrogen. After the Pd/C catalyst was filtered and the MeOH was removed under vacuum, the residue was used without further purification. To a solution of the intermediate in DMF (50.00 mL) was added Fmoc-Asp-O^{t}Bu (12.14 g, 29.56 mmol), HOBt (3.99 g, 29.56 mmol) and DIC (3.72 g, 29.56 mmol) mixture of DCM/DMF (1:1, 100.00 mL) solution. The reaction was stirred overnight at room temperature. Then, the reaction was filtrated and the filtrate was washed

successively with 1 M HCl (3×100.00 mL), saturated $NaHCO_3$ (3×100.00 mL) and brine (3×100.00 mL). The organic phase was dried over Na_2SO_4, filtered, concentrated and purified by column chromatography (100:1-50:1, DCM/MeOH) to give 4 as a white powder (14.10 g, 71.2 %, 2 steps). **^{1}H-NMR (300 MHz, $CDCl_3$):** δ 7.75 (d, *J*= 3.0 Hz, 2H), 7.60 (d, *J*= 3.0 Hz, 2H), 7.40-7.37 (m, 2H), 7.36-7.26 (m, 2H), 7.17 (s, 1H), 6.07 (s, 1H), 5.94-75.92 (m, 1H), 5.12-5.05 (m, 3H), 4.42-4.30 (m, 2H), 4.29-4.21 (m, 3H), 4.06-4.04 (m, 2H), 3.74-3.73 (m, 1H), 2.85-2.82 (m, 1H), 2.71-2.69 (m,1H), 2.56 (s, 2H), 2.06-2.03 (m, 8H), 1.96 (s, 2H), 4.42-4.30 (m, 2H), 1.44 (s, 9H). **^{13}C-NMR (300 MHz, $CDCl_3$):** δ 173.86, 173.44, 172.52, 172.07, 171.35, 170.64, 157.55, 145.34, 145.22, 142.70, 129.12, 128.49, 126.59, 121.39, 83.66, 81.74, 75.02, 74.33, 68.97, 68.60, 63.08, 54.97, 52.43, 48.57, 39.43, 29.33, 22.12, 21.99. **ESI-MS m/z** calcd for $C_{37}H_{45}N_3O_{13}$ 739.30; found $[M+H]^+$ 740.19.

*4.3.3. N^2-(((9H-fluoren-9-yl)methoxy)carbonyl)-N^4-((2R,3R,4R,5S,6R)-3-acetamido-4,5-diacetoxy-6-(acetoxymethyl)tetrahydro-2H-pyran-2-yl)asparagines (**5**)*

4 (10.0 g, 13.53 mmol) was dissolved in TFA/DCM (1:1, 20.00 mL) and stirred for 2 hours at room temperature. The reaction mixture was concentrated *in vacuo* to yield 5 as a white powder (8.77 g, 95.3 %) which was used directly in SPPS without further purification. **^{1}H-NMR (300 MHz, *d*-DMSO):** δ 8.55 (d, *J*= 6.0 Hz, 1H), 7.88-7.85 (m, 3H), 7.69 (d, *J*= 6.0 Hz, 2H), 7.47 (d, *J*= 3.0 Hz, 1H), 7.41-7.36 (m, 2H), 7.32-7.29 (m, 2H), 5.17-5.14 (m, 1H), 5.09-5.06 (m, 1H), 4.91-4.78 (m, 1H), 4.27-4.24 (m, 1H), 4.23-4.15 (m, 5H), 3.94-3.85 (m, 3H), 2.66-2.62 (m, 1H), 1.97-1.94 (m,7H), 1.88 (s, 3H), 1.70 (s, 2H). **^{13}C-NMR (300 MHz, *d*-DMSO):** δ 174.82, 171.90, 171.67, 171.37, 171.19, 157.71, 145.67, 142.56, 129.51, 128.96, 127.13, 121.99, 79.97, 75.25, 74.17, 70.28, 67.58, 65.72, 54.00, 51.87, 48.48, 38.73, 24.46, 22.40, 22.38, 22.25. **ESI-MS m/z** calcd for $C_{33}H_{37}N_3O_{13}$ 683.23; found $[M+Na]^+$ 706.54, $[M-H]^-$ 682.39.

*4.3.4. (S)-3-azido-2-((tert-butoxycarbonyl)amino)propanoic acid (**10**)*

To a solution of NaN_3 (9.75 g, 154.00 mmol) in DCM/water (2:1, 75.00 mL) was added Tf_2O (5.00 mL, 31.00 mmol) dropwise over 15 min at 0 ºC. The reaction mixture was stirred vigorously at 0 ºC for 2 hours. The organic phase was separated, washed with saturated Na_2CO_3 (3×100.00 mL) and used without further purification. To a mixture of commercially available Boc-Dap-OH (5, 3.18 g, 15.6 mmol), K_2CO_3 (4.30 g, 31.20 mmol) and $CuSO_4 \cdot 5H_2O$ (25.00 mg, 0.10 mmol) in water/MeOH (2:1, 135.00 mL) was added freshly prepared TfN_3 solution dropwise at 0 ºC, then more MeOH was added to homogeneity. The mixture was allowed to warm to room temperature and stirred overnight. The DCM and MeOH was removed under vacuum and the aqueous solution was acidified by 10 % HCl to pH=2. After dilution with EtOAc (100.00 mL), the organic layer was separated, washed with brine (3×100.00 mL), dried over Na_2SO_4, concentrated and purified by column chromatography (80:1-20:1, DCM/MeOH) to give 10 as a colorless oil (2.62 g, 73.1 %). **^{1}H-NMR (300 MHz, *d*-DMSO):** δ 7.24 (d, *J*= 6.0 Hz, 1H), 4.14 (s, 1H), 3.58 (m, 2H), 1.39 (s, 9H). **^{13}C-NMR (300 MHz, *d*-DMSO):** δ 171.32, 155.37, 78.53, 53.51, 50.94, 28.20. **ESI-MS m/z** calcd for $C_8H_{14}N_4O_4$ 230.10; found $[M-H]^-$ 229.24.

*4.3.5. allyl(S)-2-(((allyloxy)carbonyl)amino)-3-azidopropanoate (**11**)*

10 (3.00 g, 13.00 mmol) was dissolved in 4 M HCl/1,4-dioxane (30.00 mL) at 0 ºC. The reaction mixture was stirred for 3 hours at room temperature. Then the resulting mixture was filtrated and the solid was washed with EtOAc twice. After dried over vacuum, the solid was used directly in the next step. To a solution of the resulting amino acid hydrochloride and sodium carbonate (2.75 g, 26.00 mmol) in water/acetonitrile (2:1, 75.00 mL) was added allyl chloroformate (1.37 mL, 13.00 mmol) dropwise at 0 ºC. The reaction was allowed to warm to room temperature and stirred under Ar for 18 hours. The solvents were removed and the residue was diluted with dimethylformamide (DMF, 20.00 mL). Then sodium bicarbonate (1.09 g, 13.00 mmol) and allyl bromide (1.12 mL, 13.00 mmol) were added. The heterogeneous mixture was stirred for 48 hours at room temperature [additional allyl bromide

(0.56 mL, 6.50 mmol) was added at 22 hour]. The reaction was concentrated, diluted with EtOAc (100.00 mL), washed with saturated $NaHCO_3$, 0.1 M $KHSO_4$, and brine. The organic layer was dried over Na_2SO_4, filtered, concentrated and purified by column chromatography (50:1-10:1, petro ether/EtOAc) to give 11 as a yellow oil (2.43 g, 73.6 %, 3 steps). **^{1}H-NMR (300 MHz, $CDCl_3$):** δ 5.94 (m, 2H), 5.62 (d, *J*= 6.0 Hz, 1H), 5.32 (m, 4H), 4.65 (d, *J*= 6.0 Hz, 2H), 4.57 (m, 3H), 3.79 (d, *J*= 3.0 Hz, 2H). **^{13}C-NMR (300 MHz, $CDCl_3$):** δ 169.15, 155.53, 132.33, 131.06, 119.45, 118.08, 66.71, 66.11, 53.95, 52.63. **ESI-MS m/z** calcd for $C_{10}H_{14}N_4O_4$ 254.10; found $[M+H]^+$ 255.26.

*4.3.6. tert-butyl (S)-2-((((9H-fluoren-9-yl)methoxy)carbonyl)amino)pent-4-ynoate (**12**)*

To a solution of commercial available H-Pra-OH (5.00 g, 44.24 mmol) in water/1,4-dioxane (1:1, 500.00 mL) was added $NaHCO_3$ (18.58 g, 221.20 mmol) and FmocOSu (74.61 g, 221.20 mmol) successively at 0 ºC. Then the mixture was stirred overnight at room temperature. After the 1,4-dioxane was removed under vacuum, the aqueous phase was acidified with 1 M HCl to pH=1-2 and extracted with EtOAc (2×100.00 mL). The organic layer was washed with brine (3×100.00 mL), dried over Na_2SO_4 and concentrated to provide crude Fmoc-Pra-OH which was used directly without further purification. To a solution of the crude Fmoc-Pra-OH, tert-Butanol (8.10 ml, 88.48 mmol) and DMAP (1.08 g, 8.85 mmol) in DCM (500.00 mL) was added DCC (10.03 g, 48.66 mmol, solved in 500.00 mL DCM) dropwise at 0 ºC. The mixture was stirred for 1 hour at 0 ºC and 4 hours at room temperature. Then, the reaction was filtrated and the filtrates were washed successively with 1 M HCl (3×100.00 mL), saturated $NaHCO_3$ (3×100.00 mL) and brine (3×100.00 mL). The organic phase was dried over Na_2SO_4, filtered, concentrated and purified by column chromatography (50:1-10:1, petro ether/EtOAc) to give 12 as a white powder (12.11 g, 70.3 %, 2 steps). **^{1}H-NMR (300 MHz, $CDCl_3$):** δ 7.79 (m, 2H), 7.44 (m, 2H), 7.38 (m, 2H), 7.32 (m, 2H), 5.70 (d, *J*= 6.0 Hz, 1H), 4.40 (m, 3H), 4.25 (m, 1H), 2.79 (s, 2H), 1.53 (s, 9H). **^{13}C-NMR (300 MHz, $CDCl_3$):** δ 169.31, 155.61, 143.87, 143.80, 141.30, 127.73, 127.08, 125.17, 120.00, 78.56,

82.88, 71.54, 67.20, 52.65, 47.14, 27.98, 22.99. **ESI-MS m/z** calcd for $C_{24}H_{25}NO_4$ 391.17; found $[M+H]^+$ 392.35 .

*4.3.7. allyl (S)-3-(4-((S)-2-((((9H-fluoren-9-yl)methoxy)carbonyl)amino)-3-(tert-butoxy)- 3-oxopropyl)-1H-1,2,3-triazol-1-yl)-2-(((allyloxy)carbonyl)amino)propanoate (**13**)*

To a solution of 11 (100.00 mg, 0.255 mmol), 12 (64.77 mg, 0.255 mmol) and CuI (72.20 mg, 0.38 mmol) in dry DMF (1.40 mL) was added DIPEA (0.44 mL, 2.55 mmol) under Ar atmosphere. Protected from light, the reaction mixture was stirred for 14 hours at room temperature. The resulting mixture is diluted with EtOAc (100.00 mL) and water (100.00 mL). The organic phases are filtered, washed with brine, dried over Na_2SO_4, filtered, concentrated and purified by column chromatography (10:1-2:1, petro ether/EtOAc) to give 13 as a white powder (138.00 mg, 84.1 %). **^{1}H-NMR (300 MHz, $CDCl_3$):** δ 7.76 (d, *J*= 6.0 Hz, 2H), 7.61 (d, *J*= 6.0 Hz, 2H), 7.40 (t, *J*= 3.0 Hz, 2H), 7.32 (m, 3H), 5.87 (m, 2H), 5.75 (d, *J*= 6.0 Hz, 1H), 5.66 (d, *J*= 6.0 Hz, 1H), 5.30 (m, 3H), 5.28 (m, 1H), 4.84 (m, 3H), 4.76 (m, 2H), 4.66 (d, *J*= 6.0 Hz, 3H), 4.37 (d, *J*= 6.0 Hz, 2H), 4.23 (m, 1H), 3.24 (m, 2H), 1.45 (s, 9H). **^{13}C-NMR (300 MHz, $CDCl_3$):** δ 170.12, 168.43, 155.90, 155.65, 143.92, 143.84, 143.03, 141.31, 132.22, 131.06, 127.72, 127.11, 125.21, 123.40, 123.27, 119.98, 119.65, 118.17, 82.64, 67.01, 66.22, 54.15, 53.84, 50.95, 50.81, 47.16, 29.71, 28.58, 27.98. **ESI-MS m/z** calcd for $C_{34}H_{39}N_5O_8$ 645.27; found [M+Na]+ 668.51.

*4.3.8. (S)-2-((((9H-fluoren-9-yl)methoxy)carbonyl)amino)-3-(1-((S)-3-oxo-2-(((tert-pentyloxy) carbonyl)amino)-3-(((E)-prop-1-en-1-yl)oxy)propyl)-1H-1,2,3-triazol-4-yl)propanoic acid (**14**)*

13 (138.00 mg, 0.21 mmol) was dissolved in TFA/DCM (1:1, 5.00 mL) and stirred for 2 hours at room temperature. The reaction mixture was concentrated *in vacuo* to yield 14 as a white powder (120.00 mg, 95.1 %) which was used directly in SPPS without further

purification. **^{1}H-NMR (300 MHz, CD_3OD):** δ 7.78 (d, *J*= 6.0 Hz, 2H), 7.74 (m, 1H), 7.63 (m, 2H), 7.38 (t, *J*= 6.0 Hz, 2H), 7.29 (t, *J*= 6.0 Hz, 2H), 5.88 (m, 2H), 5.32 (d, *J*= 6.0 Hz, 1H), 5.24 (m, 2H), 5.13 (m, 1H), 4.83 (m, 3H), 4.72 (m, 2H), 4.64 (m, 2H), 4.48 (m, 3H), 4.32 (m, 2H), 4.20 (m, 1H), 3.29 (m, 1H). **^{13}C-NMR (300 MHz, CD_3OD):** δ 174.42, 174.32, 170.28, 158.45, 158.06, 145.26, 144.81, 144.49, 142.61, 134.08, 133.03, 128.84, 128.22, 126.33, 125.40, 120.97, 119.12, 117.78, 68.10, 67.50, 66.86, 55.61, 55.27, 55.11, 51.50, 28.82. **ESI-MS m/z** calcd for $C_{30}H_{31}N_5O_8$ 589.21; found $[M-H]^-$ 588.19.

4.3.9. General procedures for the Fmoc solid phase peptide synthesis

The amino acid residues were attached to the Rink amide resin (loading capacity= 0.33 mmol/g) with a single coupling procedure. All peptides were synthesized with a scale of 0.10 mmol.

(a) Standard pre-activation of resin protocol: The resin was swollen in DCM/DMF mixture solvent for 10 min.

(b) Standard Fmoc-deprotection protocol: After treatment with 20 % piperidine/DMF (15 min twice) the resin was washed with DMF (5×), DCM (5×), and DMF (5×).

(c) Standard coupling of natural amino acids protocol: After pre-activation of 4.00 equiv of Fmoc-protected amino acid in DMF for 5 min using 3.80 equiv of HCTU and 8.00 equiv of DIPEA, the solution was added to the resin. After 30 min, the resin was washed with DMF (5×), DCM (5×), and DMF (5×). The coupling reaction was monitored with the ninhydrin test.

(d) Standard coupling of glycoamino acid or diaminodiacid protocol: After pre-activation of 1.50 equiv of glycoamino acid or diaminodiacid building block in DMF for 15 min using 2.00 equiv of HATU, 2.00 equiv of HOAt and 8.00 equiv of DIPEA, the solution was added to the resin. After 2 hours, the resin was washed with DMF (5×), DCM (5×), and DMF (5×). The coupling reaction was monitored with the ninhydrin test.

(e) Standard capping protocol: Ac_2O/DIPEA/DMF (1:1:8) was added to the resin. After

mechanically stirring for 15 min, the resin was washed with DMF (5×) and DCM (10×)

(f) Standard deprotection of acetyl group protocol: To the peptide resin was added a solution of 10 % hydrazine hydrate/DMF solution (10 mL). The resin was stirred for 12 hours. Then, the resin was washed with DCM (5×) and DMF (5×).

(g) Standard deprotection of Alloc/allyl protocol: To the peptide resin was added a solution of 24.00 equiv of $PhSiH_3$ in 2.00 mL DCM in the presence of argon and the resin was manually stirred for 2 min. Subsequently, a solution of 0.25 equiv of $Pd(PPh_3)_4$ in 6.00 mL DCM was added. The reaction was mechanically stirred for 3 hours under argon. Then, the resin was washed with DMF (5×), DCM (5×) and DMF (5×).

(h) Standard cyclization protocol: After removal of Alloc/allyl and *N*-terminus Fmoc successively, a solution of 5.00 equiv of PyAOP, 5.00 equiv of HOAt and 10.00 equiv of NMM in NMP was added to the resin. After overnight reaction, the resin was washed with DMF (5×), DCM (5×) and DMF (5×).

(i) Standard cleavage protocol: The cleavage cocktail (TFA/TIPs/EDT/water= 95: 2: 2: 1, *v/v/v/v*) was added to the resin. After stirring for 2 hours, the cleavage cocktail was collected. The solution was bubbled with argon for concentration and the chilled diethyl ether was added to precipitate the crude peptides. The peptide suspensions were centrifuged for 3 min at 3000 rpm and then the clear solution was decanted. The step of precipitation, centrifugation and decantation operations was repeated three times. The resulting white residues were dissolved in CH_3CN/water, analyzed and purified by RP-HPLC.

(j) Standard oxidative folding protocol: Peptide in the reduced form was dissolved in the oxidation buffer [0.50 mg/mL peptide in 6.00 M guanidine hydrochloride and 100.00 mM sodium dihydrogen phosphate PBS buffer, pH=7.40, with 10.00 % dimethylsulfoxide (DMSO)]. This mixture was allowed to stir for 24 hours at room temperature. Then it was

analyzed and purified by RP-HPLC.

(k) Standard deprotection of 4-methoxybenzyl (Mob) group and oxidative folding protocol: Peptide with Mob protection was dissolved in TFA/DMSO solution (1:1, *v/v*). This mixture was allowed to stir for 20 min at room temperature. Then it was analyzed and purified by RP-HPLC.

4.4. Molecular docking

All the molecular modeling calculations were performed using SYBYL version 6.9. Structures of compounds were assigned with Gasteiger–Huckel partial atomic charges. Energy minimization was performed using the Tripos force field, Powell optimization method, and MAXIMIN 2 minimizer, with a convergence criterion of 0.001 kcal/mol Å. Simulated annealing was then performed. The system was heated to 1000 K for 1.0 ps and then annealed to 250 K for 1.5 ps. The annealing function was exponential; 50 such cycles of annealing were run and the resulting 50 conformers were optimized using methods described above. The lowest energy conformation was selected. All the other parameters were default values

4.5. Kinetic binding studies by surface plasmon resonance

Binding experiments were carried out on BiaCORE T200 (BiaCORE, Uppsala, Sweden) instruments at 25 ℃. Recombinant sRANKL were immobilized to the dextran gydrogel on the sensor surface (BiaCORE CM5 sensor chip) with a surface density of 3500 resonance units. The surface regeneration was carried out among binding cycles using Gly-HCl buffer (pH=2.5). The apparent rate constants (k_{on} and k_{off}) and the equilibrium binding constant (K_d) for the binding interaction were estimated from the kinetic analysis of sensorgrams, using the BIA evaluation software (BiaCORE).

4.6. CD spectroscopy study

CD measurements were recorded on a JASCO J-820 spectropolarimeter (JASCO Corp., Ltd). Peptides were dissolved in 50.0 % TFE aqueous solution with a concentration of 0.1 mg/mL. UV spectra were recorded at 20 ℃ in a quartz cell of 10.0 mm path length.

4.7. Immunoblotting study

RAW264.7 cells (1×10^5/well) were cultured in 6-well plates for 12 hours, treated with or without the peptides for 2 hours, and stimulated with sRANKL at 300 ng/mL for the indicated periods. Cells were then washed with PBS buffer and lysed with lysis buffer. Cell lysates (20 μg) were separated by SDS-PAGE, electroblotted onto nitrocellulose membranes and probed with anti-phospho-IκBα, anti-IκBα, anti-ERK2 antibodies (Abcam, UK). The membranes were then measured by the enhanced chemiluminescence (ECL) system.

4.8. Effect on sRANKL-induced osteoclase formation *in vitro*

Murine osteoclast precursors from 8-week-old C57BL/6 male mice were cultured in 96 well plates (1×10^5/mL, 200 μL/well) for 3 days co-cultured with 30 ng/mL murine CSF-1 and 300 ng/mL sRANKL with or without treatment of designed peptides at the indicated concentration. Then, the fixed cells were stained using tartrate-resistant acid phosphatase kit (TRAP kit, Sigma). TRAP-positive multinucleated cells (with more than three nuclei) were observed and counted by a microscope (OLYMPUS-BX53).

4.9. CCK-8 assay

The CCK-8 assay was performed according to the manufacturer's instructions. The CCK-8 reagent (Sigma) was dissolved with PBS solution in a concentration of 5 mg/mL. BMMCs were cultured on a 96-well plate (1×10^5/mL, 100 μL/well) for 24 hours incubation. Cells were then cultured with various concentrations of OM-1, OM-2, OM-3 and OM-4 (0, 12.5, 25.0, 50.0, 100.0 μM) for 48 hours. The CCK-8 solution was added at 10 μL per well and incubated for 2 hours. Absorbance was measured at 450 nm using ELISA plate reader.

4.10. *In vivo* experiments

All experiments were performed in the SPF laboratory of Changhai Hospital, Shanghai. Female 6-week-old C57BL/6 mice were supplied by Slack (Shanghai, China). All animal

procedures were in accordance with the standards of the Ethics Committee at Second Military Medical University. We divided the mice into three groups of six mice each: a control group; ovariectomized mice treated with saline (OVX group); and OVX mice treated with OM-2 dissolved in saline (OVX+OM-2 group). The treated mice were injected intraperitoneally (i.p.) with 20.0 mg/kg of OM-2 or vehicle every day. After 6 weeks of intervention, all mice were anesthetized with chloral hydrate. Samples of femur bone and blood were obtained. Blood was centrifuged with 3000 r for 5 minutes to give the supernatant, which was stored at -80 ^{o}C. Finally, the mice were euthanized.

4.11. Bone histomorphometry analysis

Femur bones were fixed with 4 % paraformaldehyde for 4 days, and then decalcified for 2 weeks using 10% tetrasodium-EDTA. Paraffin-embedded sections (4 μm) from each femur were processed for histologic observation of the metaphysis below the spongiosa by hematoxylin and eosin (H&E) staining, and TRAP staining. Histologic measurements and images were observed by a microscope (OLYMPUS-BX53). Trabecular bone was shown in the H&E-stained sections, and its area was measured by Image-Pro Plus software. The numbers of osteoclasts in the region of the metaphysis were counted within the sections by TRAP staining.

4.12. Bone structure analysis

The femur bone structure was analyzed by micro-computed tomography (Micro CT) (Huaiyu biological technology limited company, Shanghai, China). Structural parameters for the metaphyseal region and the trabecular bone were analyzed using the built-in software of the Micro CT. The evaluated trabecular parameters were total bone mineral density (BMD), bone volume expressed per unit total volume (BV/TV), trabecular number (Tb. N) and bone surface area expressed per unit total volume (BS/TV).The built-in software was used to reconstruct two-dimensional and three-dimensional bone structure images.

4.13. Serum biochemistry

Serum was collected by the above methods. Serum levels of IL-6, TRAPcp5B, CTX-1 and TNF-α were measured using ELISA kits (Anogen, Canada), according to the manufacturer's instructions.

Acknowledgements

We are grateful to the National Natural Science Foundation of China (No. 21402235, 31370958 and 81461148033), PLA Youth Medical Science and Technology Youth Development Program (No.16QNP086), and Instrumental Analysis Center of our university for NMR spectroscopic and mass spectrometric analyses.

Conflict of Interest: The authors have no conflicts of interest to disclose.

References:

[1] J.R. Edwards, G.R. Mundy, Advances in osteoclast biology: old findings and new insights from mouse models, Nat. Rev. Rheumatol. 7 (2011) 235-243.
[2] S. Ochi, M. Shinohara, K. Sato, H.J. Gober, T. Koga, T. Kodama, T. Takai, N. Miyasaka, H. Takayanagi, Pathological role of osteoclast costimulation in arthritis-induced bone loss, Proc. Natl. Acad. Sci. U. S. A. 104 (2007) 11394-11399.
[3] NIH Consensus Development Panel on Osteoporosis Prevention, Diagnosis, and Therapy, March 7-29, 2000: highlights of the conference, South. Med. J. 94 (2001) 569-573.
[4] J.A. Kanis, Assessment of fracture risk and its application to screening for postmenopausal osteoporosis: synopsis of a WHO report. WHO Study Group, Osteoporos. Int. 4 (1994) 368-381.
[5] M. Kawatani, H. Okumura, K. Honda, N. Kanoh, M. Muroi, N. Dohmae, M. Takami, M. Kitagawa, Y. Futamura, M. Imoto, H. Osada, The identification of an osteoclastogenesis inhibitor through the inhibition of glyoxalase I, Proc. Natl. Acad. Sci. U. S. A. 105 (2008) 11691-11696.
[6] B. Ettinger, D.M. Black, B.H. Mitlak, R.K. Knickerbocker, T. Nickelsen, H.K. Genant, C. Christiansen, P.D. Delmas, J.R. Zanchetta, J. Stakkestad, C.C. Gluer, K. Krueger, F.J. Cohen, S. Eckert, K.E. Ensrud, L.V. Avioli, P. Lips, S.R. Cummings, Reduction of vertebral fracture risk in postmenopausal women with osteoporosis treated with raloxifene: results from a 3-year randomized clinical trial. Multiple Outcomes of Raloxifene Evaluation (MORE) Investigators, Jama 282 (1999) 637-645.
[7] M. Hiligsmann, O. Bruyere, J.Y. Reginster, Cost-utility of long-term strontium ranelate treatment for postmenopausal osteoporotic women, Osteoporos. Int. 21 (2010) 157-165.
[8] R.M. Neer, C.D. Arnaud, J.R. Zanchetta, R. Prince, G.A. Gaich, J.Y. Reginster, A.B. Hodsman, E.F. Eriksen, S. Ish-Shalom, H.K. Genant, O. Wang, B.H. Mitlak, Effect of parathyroid hormone (1-34) on fractures and bone mineral density in postmenopausal women with osteoporosis, N. Engl. J. Med. 344 (2001) 1434-1441.
[9] S. Boonen, F. Marin, D. Mellstrom, L. Xie, D. Desaiah, J.H. Krege, C.J. Rosen, Safety and efficacy of teriparatide in elderly women with established osteoporosis: bone anabolic therapy from a geriatric perspective, J. Am. Geriatr. Soc. 54 (2006) 782-789.

[10] P.D. Delmas, L. van de Langerijt, N.B. Watts, R. Eastell, H. Genant, A. Grauer, D.L. Cahall, Underdiagnosis of vertebral fractures is a worldwide problem: the IMPACT study, J. Bone Miner. Res. 20 (2005) 557-563.
[11] M.J. Panneman, P. Lips, S.S. Sen, R.M. Herings, Undertreatment with anti-osteoporotic drugs after hospitalization for fracture, Osteoporos. Int. 15 (2004) 120-124.
[12] B.F. Boyce, L. Xing, Functions of RANKL/RANK/OPG in bone modeling and remodeling, Arch. Biochem. Biophys. 473 (2008) 139-146.
[13] L.E. Theill, W.J. Boyle, J.M. Penninger, RANK-L and RANK: T cells, bone loss, and mammalian evolution, Annu. Rev. Immunol. 20 (2002) 795-823.
[14] S. Theoleyre, Y. Wittrant, S.K. Tat, Y. Fortun, F. Redini, D. Heymann, The molecular triad OPG/RANK/RANKL: involvement in the orchestration of pathophysiological bone remodeling, Cytokine Growth Factor Rev. 15 (2004) 457-475.
[15] W.C. Dougall, M. Glaccum, K. Charrier, K. Rohrbach, K. Brasel, T. De Smedt, E. Daro, J. Smith, M.E. Tometsko, C.R. Maliszewski, A. Armstrong, V. Shen, S. Bain, D. Cosman, D. Anderson, , P.J. Morrissey, J.J. Peschon, J. Schuh, RANK is essential for osteoclast and lymph node development, Genes Dev. 13 (1999) 2412-2424.
[16] Y.Y. Kong, H. Yoshida, I. Sarosi, H.L. Tan, E. Timms, C. Capparelli, S. Morony, A.J. Oliveira-dos-Santos, G. Van, A. Itie, W. Khoo, A. Wakeham, C.R. Dunstan, D.L. Lacey, T.W. Mak, W.J. Boyle, J.M. Penninger, OPGL is a key regulator of osteoclastogenesis, lymphocyte development and lymph-node organogenesis, Nature 397 (1999) 315-323.
[17] J. Li, I. Sarosi, X.Q. Yan, S. Morony, C. Capparelli, H.L. Tan, S. McCabe, R. Elliott, S. Scully, G. Van, S. Kaufman, S.C. Juan, Y. Sun, J. Tarpley, L. Martin, K. Christensen, J. McCabe, P. Kostenuik, H. Hsu, F. Fletcher, C.R. Dunstan, D.L. Lacey, W.J. Boyle, RANK is the intrinsic hematopoietic cell surface receptor that controls osteoclastogenesis and regulation of bone mass and calcium metabolism, Proc. Natl. Acad. Sci. U. S. A. 97 (2000) 1566-1571.
[18] W.S. Simonet, D.L. Lacey, C.R. Dunstan, M. Kelley, M.S. Chang, R. Luthy, , H.Q. Nguyen, S. Wooden, L. Bennett, T. Boone, G. Shimamoto, M. DeRose, R. Elliott, A. Colombero, H.L. Tan, G. Trail, J. Sullivan, E. Davy, N. Bucay, L. Renshaw-Gegg, T.M. Hughes, D. Hill, W. Pattison, P. Campbell, S. Sander, G. Van, J. Tarpley, P. Derby, R. Lee, W. J. Boyle, Osteoprotegerin: a novel secreted protein involved in the regulation of bone density, Cell 89 (1997) 309-319.
[19] H. Yasuda, N. Shima, N. Nakagawa, K. Yamaguchi, M. Kinosaki, S. Mochizuki, A. Tomoyasu, K. Yano, M. Goto, A. Murakami, E. Tsuda, T. Morinaga, K. Higashio, N. Udagawa, N. Takahashi, T. Suda, Osteoclast differentiation factor is a ligand for osteoprotegerin/osteoclastogenesis-inhibitory factor and is identical to TRANCE/RANKL, Proc. Natl. Acad. Sci. U. S. A. 95 (1998) 3597-3602.
[20] P.K. Anaraki, M. Patecki, S. Tkachuk, Y. Kiyan, H. Haller, I. Dumler, Urokinase Receptor Mediates Osteoclastogenesis via M-CSF Release From Osteoblasts and the c-Fms/PI3K/Akt/NF-kappa B Pathway in Osteoclasts, J. Bone Miner. Res. 30 (2015) 379-388.
[21] T. Michigami, M. Ihara-Watanabe, M. Yamazaki, K. Ozono, Receptor activator of nuclear factor kappaB ligand (RANKL) is a key molecule of osteoclast formation for bone metastasis in a newly developed model of human neuroblastoma, Cancer Res. 61 (2001) 1637-1644.
[22] D.M. Anderson, E. Maraskovsky, W.L. Billingsley, W.C. Dougall, M.E. Tometsko, E.R. Roux, M.C. Teepe, R.F. DuBose, D. Cosman, L. Galibert, A homologue of the TNF receptor and its ligand enhance T-cell growth and dendritic-cell function, Nature 390 (1997) 175-179.
[23] B.G. Darnay, V. Haridas, J. Ni, P.A. Moore, B.B. Aggarwal, Characterization of the intracellular domain of receptor activator of NF-kappaB (RANK). Interaction with tumor necrosis factor receptor-associated factors and activation of NF-kappab and c-Jun N-terminal kinase, J. Biol. Chem. 273 (1998) 20551-20555.
[24] H. Hsu, D.L. Lacey, C.R. Dunstan, I. Solovyev, A. Colombero, E. Timms, H.L. Tan, G. Elliott, M.J. Kelley, I. Sarosi, L. Wang, X.Z. Xia, R. Elliott, L. Chiu, T. Black, S. Scully, C. Capparelli, S.G. Morony, Shimamoto, M.B. Bass, W.J. Boyle, Tumor necrosis factor receptor

family member RANK mediates osteoclast differentiation and activation induced by osteoprotegerin ligand, Proc. Natl. Acad. Sci. U. S. A. 96 (1999) 3540-3545.
[25] B. Bolon, G. Campagnuolo, U. Feige, Duration of bone protection by a single osteoprotegerin injection in rats with adjuvant-induced arthritis, Cell Mol. Life Sci. 59 (2002) 1569-1576.
[26] M.L. Bouxsein, Determinants of skeletal fragility, Best Pract. Res. Clin. Rheumatol. 19 (2005), 897-911.
[27] D. Felsenberg, S. Boonen, The bone quality framework: determinants of bone strength and their interrelationships, and implications for osteoporosis management, Clin. Ther. 27 (2005) 1-11.
[28] E. Seeman, P.D. Delmas, Bone quality--the material and structural basis of bone strength and fragility, N. Engl. J. Med. 354 (2006) 2250-2261.
[29] A.P. Anandarajah, Role of RANKL in bone diseases, Trends Endocrinol. Metab. 20 (2009) 88-94.
[30] A.E. Kearns, S. Khosla, P.J. Kostenuik, Receptor activator of nuclear factor kappaB ligand and osteoprotegerin regulation of bone remodeling in health and disease, Endocr. Rev. 29 (2008), 155-192.
[31] S. Tanaka, Signaling axis in osteoclast biology and therapeutic targeting in the RANKL/RANK/OPG system, Am. J. Nephrol. 27 (2007) 466-478.
[32] S. Tanaka, K. Nakamura, N. Takahasi, T. Suda, Role of RANKL in physiological and pathological bone resorption and therapeutics targeting the RANKL-RANK signaling system, Immunol. Rev. 208 (2005) 30-49.
[33] K. Vanderkerken, E. De Leenheer, C. Shipman, K. Asosingh, A. Willems, B. Van Camp, P. Croucher, Recombinant osteoprotegerin decreases tumor burden and increases survival in a murine model of multiple myeloma, Cancer Res. 63 (2003) 287-289.
[34] B.T. Feeley, N.Q. Liu, A.H. Conduah, L. Krenek, K. Roth, W.C. Dougall, J. Huard, S. Dubinett, J. R. Lieberman, Mixed metastatic lung cancer lesions in bone are inhibited by noggin overexpression and Rank:Fc administration, J. Bone Miner. Res. 21 (2006) 1571-1580.
[35] S.R. Cummings, J. San Martin, M.R. McClung, E.S. Siris, R. Eastell, I.R. Reid, P. Delmas, H.B. Zoog, M. Austin, A. Wang, S. Kutilek, S. Adami, J. Zanchetta, C. Libanati, S. Siddhanti, C. Christiansen, Denosumab for prevention of fractures in postmenopausal women with osteoporosis, N. Engl. J. Med. 361 (2009) 756-765.
[36] A. Lipton, G.G. Steger, J. Figueroa, C. Alvarado, P. Solal-Celigny, J.J. Body, R. de Boer, , R. Berardi, P. Gascon, K.S. Tonkin, R. Coleman, A.H. Paterson, M.C. Peterson, M. Fan, A. Kinsey, S. Jun, Randomized active-controlled phase II study of denosumab efficacy and safety in patients with breast cancer-related bone metastases, J. Clin. Oncol. 25 (2007) 4431-4437.
[37] S.B. Cohen, R.K. Dore, N.E. Lane, P.A. Ory, C.G. Peterfy, J.T. Sharp, D. van der Heijde, L. Zhou,W. Tsuji, R. Newmark, Denosumab treatment effects on structural damage, bone mineral density, and bone turnover in rheumatoid arthritis: a twelve-month, multicenter, randomized, double-blind, placebo-controlled, phase II clinical trial, Arthritis Rheum. 58 (2008) 1299-1309.
[38] J.P. Brown, R.L. Prince, C. Deal, R.R. Recker, D.P. Kiel, L.H. de Gregorio, P. Hadji, L.C. Hofbauer, J.M. Alvaro-Gracia, H. Wang, M. Austin, R.B. Wagman, R. Newmark, C. Libanati, J. San Martin, H. G. Bone, Comparison of the effect of denosumab and alendronate on BMD and biochemical markers of bone turnover in postmenopausal women with low bone mass: a randomized, blinded, phase 3 trial, J. Bone Miner. Res. 24 (2009) 153-161.
[39] E.M. Lewiecki, RANK ligand inhibition with denosumab for the management of osteoporosis, Expert Opin. Biol. Ther. 6 (2006) 1041-1050.
[40] N. Setsu, E. Kobayashi, N. Asano, N. Yasui, H. Kawamoto, A. Kawai, K. Horiuchi, Severe hypercalcemia following denosumab treatment in a juvenile patient, J. Bone Miner. Metab. 34 (2016) 118-122.

[41] P. Yerram, S. Kansagra, O. Abdelghany, Incidence of hypocalcemia in patients receiving denosumab for prevention of skeletal-related events in bone metastasis, J. Oncol. Pharm. Pract. 23 (2017) 179-184.
[42] H.M. Ta, G.T. Nguyen, H.M. Jin, J. Choi, H. Park, N. Kim, H.Y. Hwang, K.K. Kim, Structure-based development of a receptor activator of nuclear factor-kappaB ligand (RANKL) inhibitor peptide and molecular basis for osteopetrosis, Proc. Natl. Acad. Sci. U. S. A. 107 (2010) 20281-20286.
[43] K. Fosgerau, T. Hoffmann, Peptide therapeutics: current status and future directions, Drug Discov. Today 20 (2015) 122-128.
[44] J. M. Mason, Design and development of peptides and peptide mimetics as antagonists for therapeutic intervention, Future Med. Chem. 2 (2010) 1813-1822.
[45] K. Aoki, H. Saito, C. Itzstein, M. Ishiguro, T. Shibata, R. Blanque, A.H. Mian, M. Takahashi, Y. Suzuki, M. Yoshimatsu, A. Yamaguchi, P. Deprez, P. Mollat, R. Murali, K. Ohya, W.C. Horne, R. Baron, A TNF receptor loop peptide mimic blocks RANK ligand-induced signaling, bone resorption, and bone loss, J. Clin. Invest. 116 (2006) 1525-1534.
[46] X. Cheng, M. Kinosaki, M. Takami, Y. Choi, H. Zhang, R. Murali, Disabling of receptor activator of nuclear factor-κB (RANK) receptor complex by novel osteoprotegerin-like peptidomimetics restores bone loss in vivo, J. Biol. Chem. 279 (2004) 8269-8277.
[47] D.J. Heath, K. Vanderkerken, X. Cheng, O. Gallagher, M. Prideaux, R. Murali, P.I. Croucher, An osteoprotegerin-like peptidomimetic inhibits osteoclastic bone resorption and osteolytic bone disease in myeloma, Cancer Res. 67 (2007) 202-208.
[48] V.G. Naidu, K.R. Dinesh Babu, M.M. Thwin, R.L. Satish, P.V. Kumar, P. Gopalakrishnakone, RANKL targeted peptides inhibit osteoclastogenesis and attenuate adjuvant induced arthritis by inhibiting NF-kappaB activation and down regulating inflammatory cytokines, Chem. Biol. Interact. 203 (2013) 467-479.
[49] X. Luan, Q. Lu, Y. Jiang, S. Zhang, Q. Wang, H. Yuan, W. Zhao, J. Wang, X. Wang, Crystal structure of human RANKL complexed with its decoy receptor osteoprotegerin, J. Immunol. 189 (2012) 245-252.
[50] D.L. Rabenstein, K.H. Weaver, Kinetics and Equilibria of the Thiol/Disulfide Exchange Reactions of Somatostatin with Glutathione, J. Org. Chem. 61 (1996) 7391-7397.
[51] H.F. Gilbert, Thiol/disulfide exchange equilibria and disulfide bond stability, Methods Enzymol. 251 (1995) 8-28.
[52] R. Kowalczyk, P.W. Harris, M.A. Brimble, K.E. Callon, M. Watson, J. Cornish, Synthesis and evaluation of disulfide bond mimetics of amylin-(1-8) as agents to treat osteoporosis, Bioorg. Med. Chem. 20 (2012) 2661-2668.
[53] H. Hu, J. Xue, B. M. Swarts, Q. Wang, Q. Wu, Z. Guo, Synthesis and antibacterial activities of N-glycosylated derivatives of tyrocidine A, a macrocyclic peptide antibiotic, J. Med. Chem. 52 (2009) 2052-2059.
[54] S.K. Tat, J.P. Pelletier, J. Verges, D. Lajeunesse, E. Montell, H. Fahmi, M. Lavigne, J. Martel-Pelletier, Chondroitin and glucosamine sulfate in combination decrease the pro-resorptive properties of human osteoarthritis subchondral bone osteoblasts: a basic science study, Arthritis. Res. Ther. 9 (2007) R117.
[55] S. Pegoraro, S. Fiori, S. Rudolph-Bohner, T.X. Watanabe, L. Moroder, Isomorphous replacement of cystine with selenocystine in endothelin: oxidative refolding, biological and conformational properties of [Sec3, Sec11, Nle7]-endothelin-1, J. Mol. Biol. 284 (1998) 779-792.
[56] K. Medini, P.W.R. Harris, A. Menorca, K. Hards, G.M. Cook, M.A. Brimble, Synthesis and activity of a diselenide bond mimetic of the antimicrobial protein caenopore-5, Chem. Science 7 (2016) 2005-2010.
[57] Y. Guo, C. Liu, H. Song, F. Wang, Y. Zou, Q. Wu, H. Hu, Diaminodiacid-based synthesis of macrocyclic peptides using 1,2,3-triazole bridges as disulfide bond mimetics, RSC Adv. 7 (2017) 2110-2114.
[58] M. Karin, A. Lin, NF-kappaB at the crossroads of life and death, Nat. Immunol. 3 (2002) 221-227.

[59] Y. Wu, Y.H. Li, X. Li, Y. Zou, H.L. Liao, L. Liu, Y.G. Chen, D. Bierer, H.G. Hu, A novel peptide stapling strategy enables the retention of ring-closing amino acid side chains for the Wnt/β-catenin signalling pathway, Chem. Science (2017) 10.1039/C7SC02420G
[60] C.A. Nelson, J.T. Warren, M.W. Wang, S.L. Teitelbaum, D.H. Fremont, RANKL employs distinct binding modes to engage RANK and the osteoprotegerin decoy receptor, Structure 20 (2012) 1971-1982.
[61] K.C. Nicolaou, C.N. Boddy, S. Brase, N. Winssinger, Chemistry, Biology, and Medicine of the Glycopeptide Antibiotics, Angew. Chem., Int. Ed. Engl. 38 (1999) 2096-2152.
[62] D. Kahne, C. Leimkuhler, W. Lu, C. Walsh, Glycopeptide and lipoglycopeptide antibiotics, Chem. Rev. 105 (2005) 425-448.
[63] S.B. Ferreira, A.C.R. Sodero, M.F.C. Cardoso, E.S. Lima, C.R. Kaiser, F.P. Silva, V.F. Ferreira, Synthesis, biological activity, and molecular modeling studies of 1H-1,2,3-triazole derivatives of carbohydrates as alpha-glucosidases inhibitors, J. Med. Chem. 53 (2010) 2364-2375.
[64] F.d.C. da Silva, M.C.B.V. de Souza, I.I.P. Frugulhetti, H.C. Castro, S.L.d.O. Souza, T.M.L. de Souza, D.Q. Rodrigues, A.M.T. Souza, P.A. Abreu, F. Passamani, C.R. Rodrigues, V. F. Ferreira, Synthesis, HIV-RT inhibitory activity and SAR of 1-benzyl-1H-1,2,3-triazole derivatives of carbohydrates, Eur. J. Med. Chem. 44 (2009) 373-383.
[65] E.R. Brandt, K.S. Sriprakash, R.I. Hobb, W.A. Hayman, W. Zeng, M.R. Batzloff, D.C. Jackson, M.F. Good, New multi-determinant strategy for a group A streptococcal vaccine designed for the Australian Aboriginal population, Nat. Med. 6 (2000) 455-459.
[66] B.L. Wilkinson, L.F. Bornaghi, S.A. Poulsen, T.A. Houston, Synthetic utility of glycosyl triazoles in carbohydrate chemistry, Tetrahedron 62 (2006) 8115-8125.
[67] K. Holland-Nell, M. Meldal, Maintaining biological activity by using triazoles as disulfide bond mimetics, Angew. Chem., Int. Ed. Engl. 50 (2011) 5204-5206.
[68] M. Empting, O. Avrutina, R. Meusinger, S. Fabritz, M. Reinwarth, M. Biesalski, S. Voigt, G. Buntkowsky, H. Kolmar, "Triazole bridge": disulfide-bond replacement by ruthenium-catalyzed formation of 1,5-disubstituted 1,2,3-triazoles, Angew. Chem., Int. Ed. Engl. 50 (2011) 5207-5211.
[69] J. Kikuta, M. Ishii, Osteoclast migration, differentiation and function: novel therapeutic targets for rheumatic diseases, Rheumatology 52 (2013) 226-234.
[70] Y.S. Park, J.Y. Lee, J.S. Suh, Y.M. Jin, Y. Yu, H.Y. Kim, Y.J. Park, C.P. Chung, I. Jo, Selective osteogenesis by a synthetic mineral inducing peptide for the treatment of osteoporosis, Biomaterials 35 (2014) 9747-9754.

Figure Legends:

Figure 1. Amino acid sequence of OPG mimics. X=Seleno-L-cysteine.

Scheme 1. A) Synthetic route of building block 5. Reagents and conditions: a) i) acetyl chloride, rt, 4 days, ii) NaN_3, tetrabutylammonium iodide, DCM/Water, rt, 1 h, 82.4 % in 2 steps; b) i) H_2, Pd/C, rt, 12 h, ii) Fmoc-Asp-O^{t}Bu, HOBt, DIC, DCM/DMF, rt, 12 h, 71.2 % in 2 steps; c) DCM/TFA (3:1, *v/v*), rt, 2 h, 95.3 %; B) Synthetic route of building block 14. Reagent and conditions: a) TfN_3, $CuSO_4 \cdot 5H_2O$, K_2CO_3, water/MeOH/CH_2Cl_2, rt, overnight, 73.1 %; b) i) 4 M HCl/1,4-dioxane, 0℃, 3 h; ii) Alloc-Cl, Na_2CO_3, water/CH_3CN, rt, 18 h; iii) allyl bromide, $NaHCO_3$, DMF, rt, 48 h, 73.6 % in 3 steps; c) i) Fmoc-OSu, Na_2CO_3, water/ 1,4-dioxane, rt, overnight; ii) ^{t}BuOH, DCC, DMAP, DCM, rt, 4 h, 70.3 % in 2 steps; d) CuI, DIPEA, DMF, rt, 14 h, 84.1 %; e) TFA/DCM (3:1, *v/v*), rt, 2 h, 95.1 %.

Scheme 2. Solid-phase synthesis route of the OPG mimics. a) i) 20 % piperidine/DMF, rt, 15 min twice; ii) Fmoc-AA-OH, HCTU, DIPEA, DMF, rt, 30 min; iii) 20 % piperidine/DMF, rt, 15 min twice; iv) Ac_2O/DIPEA/DMF, rt, 15 min; b) i) TFA/EDT/TIPs/water (95:2:2:1, *v/v/v/v*), rt, 2 h; c) 6 M Gn·HCl/100 mM Na_2HPO_4 PBS buffer (pH=7.4), 10 % DMSO, open flask, rt, 24 h; d) i) 20 % piperidine/DMF, rt, 15 min twice; ii) Fmoc-AA-OH, HCTU, DIPEA, DMF, rt, 30 min; iii) 20 % piperidine/DMF, rt, 15 min twice; iv) **5**, HATU, HOAt, DIPEA, DMF, rt, 2 h; v) 20 % piperidine/DMF, rt, 15 min twice; vi) Ac_2O/DIPEA/DMF, rt, 15 min; e) i) 10 % hydrazine hydrate/DMF, rt, 12 h, f) i) TFA/EDT/TIPs/water (95:2:2:1, *v/v/v*), rt, 2 h; ii) 6 M Gn·HCl/100 mM Na_2HPO_4 PBS buffer (pH=7.4), 10 % DMSO, open flask, rt, 24 h; g) i) 20 % piperidine/DMF, rt, 15 min twice; ii) Fmoc-AA-OH, HCTU, DIPEA, DMF, rt, 30 min; iii) 20 % piperidine/DMF, rt, 15 min twice; iv) Ac_2O/DIPEA/DMF, rt, 15 min; h) TFA/EDT/TIPs/water (95:2:2:1, *v/v/v/v*), rt, 2 h; i) 50 % TFA/DMSO, rt, 20 min; j) i) 20 % piperidine/DMF, rt, 15 min twice; ii) Fmoc-AA-OH, HCTU, DIPEA, DMF, rt, 30 min; iii) 20 % piperidine/DMF, rt, 15 min twice; iv) **14**, HATU, HOAt, DIPEA, DMF, rt, 2 h; k) $Pd(PPh_3)_4$, $PhSiH_3$, DCM, rt, 3 h; ii) 20 % piperidine/DMF, rt, 10 min; iii) PyAOP, HOAt, NMM, NMP, rt, 12 h; iv) Ac_2O/DIPEA/DMF, rt, 15 min; l) TFA/EDT/TIPs/Water (95:2:2:1, *v/v/v/v*), rt, 2 h; The resin-bound peptides were protected on side chains at asterisk sites. The following protecting groups for amino acid side chains were used: tert-butyl (^{t}Bu; for Tyr and Glu), 2,2,4,6,7-pentamethyldihydrobenzo-furane-5-sulfonyl (pbf; for Arg), tert-butyloxycarbonyl (Boc; for Lys) and trityl (Trt; for Cys), 4-methoxybenzyl (Mob; for Sec).

Figure 2. A) Inhibitory effects of OPG mimics on the sRANKL-induced osteoclast differentiation, estimated by the number of TRAP-positive multinucleated cells. B) Dose-dependent inhibition of OM-2 and OP3-4 on the sRANKL-induced osteoclast differentiation estimated by the number of TRAP-positive multinucleated cells. The results represent the mean value SEM of three independent experiments.

Figure 3. A) CD spectra of the peptides in 50% TFE aqueous solution at 20 °C. B) SPR binding studies of OM-2 to RANKL. C) SPR binding studies of OM-1 to RANKL. D) Effects of OM-2 and OP3-4 treatment on down-stream NF-κB signaling pathway by western blot. E) Proteolytic stability of OM-1 *vs.* OM-2 under α-chymotrypsin treatment. Data points are displayed as the mean value SEM of duplicate independent experiments. The percent residual peptide was monitored *via* HPLC.

Figure 4. OM-2 reduces ovariectomy-induced bone loss *in vivo*. A) Representative H&E staining of distal femoral sections and quantification of trabecular area. B) Representative

TRAP-stained histologic distal femur sections from sham, OVX and OVX + OM-2 group. C) Micro CT analysis of the distal femur from sham, OVX, and OVX + OM-2 group. D) Calculations of trabecular number (Tb.N), bone surface area/ tissue volume (BS/TV), bone volume / tissue volume (BV/TV) and bone mineral density (BMD). E) Serum IL-6, TNF-α, TRAcp 5B and CTX-1 were examined (*P < 0.05, **P < 0.01, ***P < 0.001).

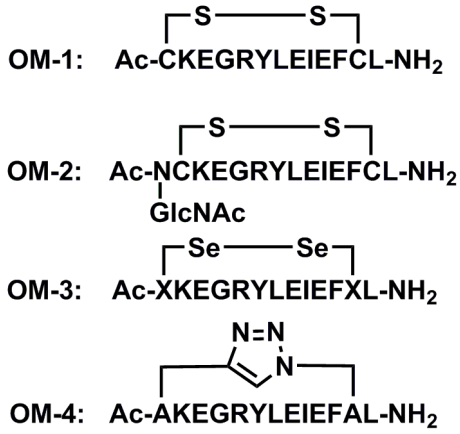

Figure 1. Amino acid sequence of OPG mimics. X=Seleno-L-cysteine.

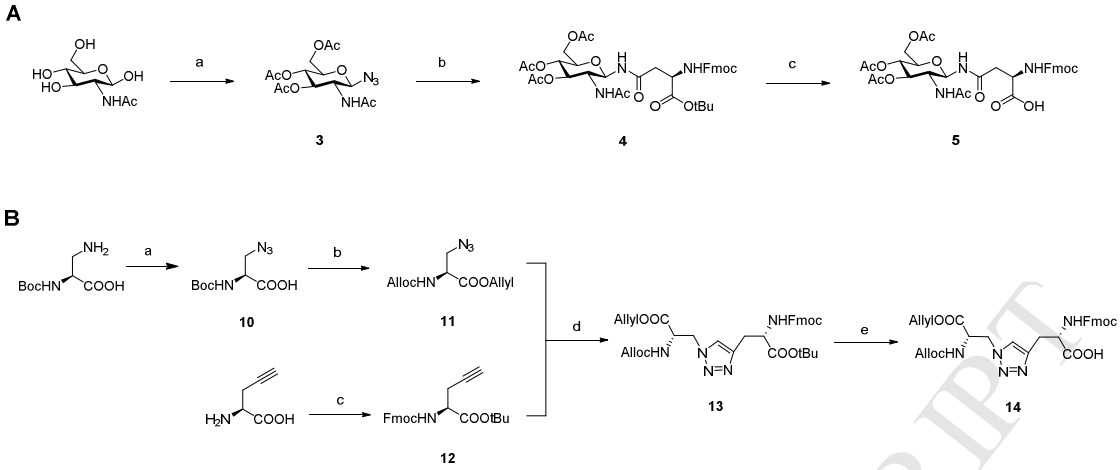

Scheme 1. A) Synthetic route of building block 5. Reagents and conditions: a) i) acetyl chloride, rt, 4 days, ii) NaN_3, tetrabutylammonium iodide, DCM/Water, rt, 1 h, 82.4 % in 2 steps; b) i) H_2, Pd/C, rt, 12 h, ii) Fmoc-Asp-O^{t}Bu, HOBt, DIC, DCM/DMF, rt, 12 h, 71.2 % in 2 steps; c) DCM/TFA (3:1, *v/v*), rt, 2 h, 95.3 %; B) Synthetic route of building block 14. Reagent and conditions: a) TfN_3, $CuSO_4 \cdot 5H_2O$, K_2CO_3, water/MeOH/CH_2Cl_2, rt, overnight, 73.1 %; b) i) 4 M HCl/1,4-dioxane, 0℃, 3 h; ii) Alloc-Cl, Na_2CO_3, water/CH_3CN, rt, 18 h; iii) allyl bromide, $NaHCO_3$, DMF, rt, 48 h, 73.6 % in 3 steps; c) i) Fmoc-OSu, Na_2CO_3, water/ 1,4-dioxane, rt, overnight; ii) ^{t}BuOH, DCC, DMAP, DCM, rt, 4 h, 70.3 % in 2 steps; d) CuI, DIPEA, DMF, rt, 14 h, 84.1 %; e) TFA/DCM (3:1, *v/v*), rt, 2 h, 95.1 %.

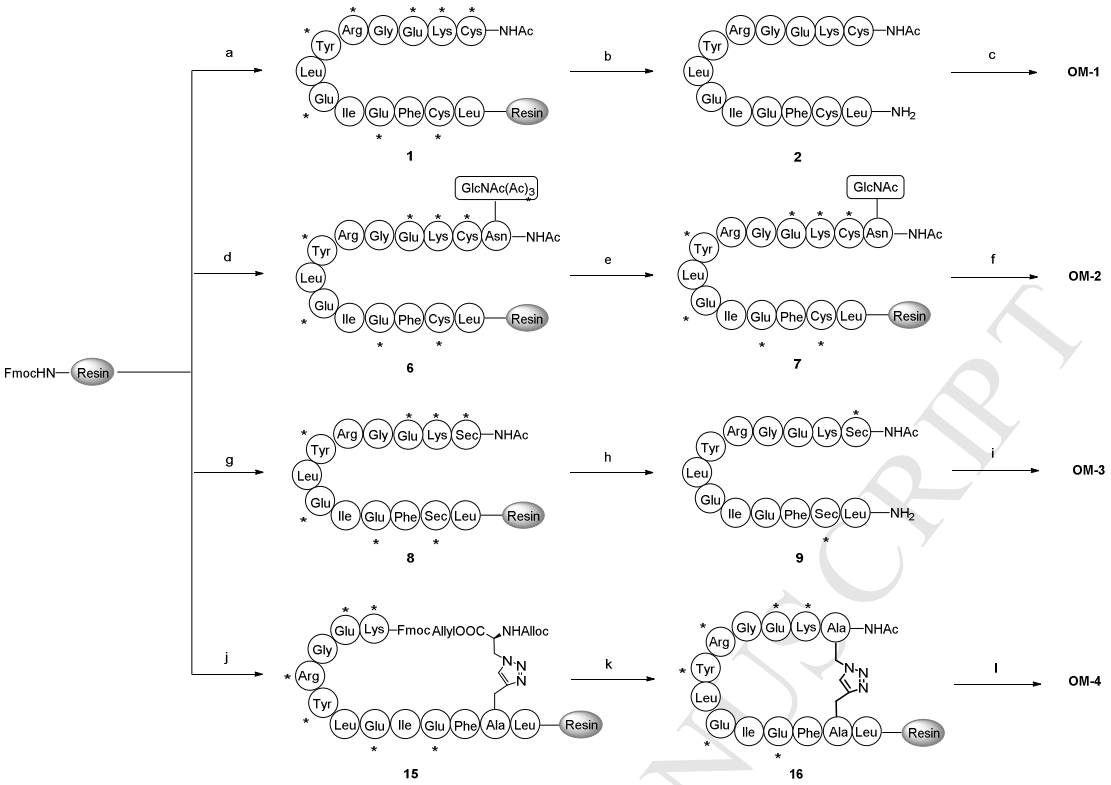

Scheme 2. Solid-phase synthesis route of the OPG mimics. a) i) 20 % piperidine/DMF, rt, 15 min twice; ii) Fmoc-AA-OH, HCTU, DIPEA, DMF, rt, 30 min; iii) 20 % piperidine/DMF, rt, 15 min twice; iv) Ac_2O/DIPEA/DMF, rt, 15 min; b) i) TFA/EDT/TIPs/water (95:2:2:1, *v/v/v/v*), rt, 2 h; c) 6 M Gn·HCl/100 mM Na_2HPO_4 PBS buffer (pH=7.4), 10 % DMSO, open flask, rt, 24 h; d) i) 20 % piperidine/DMF, rt, 15 min twice; ii) Fmoc-AA-OH, HCTU, DIPEA, DMF, rt, 30 min; iii) 20 % piperidine/DMF, rt, 15 min twice; iv) **5**, HATU, HOAt, DIPEA, DMF, rt, 2 h; v) 20 % piperidine/DMF, rt, 15 min twice; vi) Ac_2O/DIPEA/DMF, rt, 15 min; e) i) 10 % hydrazine hydrate/DMF, rt, 12 h, f) i) TFA/EDT/TIPs/water (95:2:2:1, *v/v/v/v*), rt, 2 h; ii) 6 M Gn·HCl/100 mM Na_2HPO_4 PBS buffer (pH=7.4), 10 % DMSO, open flask, rt, 24 h; g) i) 20 % piperidine/DMF, rt, 15 min twice; ii) Fmoc-AA-OH, HCTU, DIPEA, DMF, rt, 30 min; iii) 20 % piperidine/DMF, rt, 15 min twice; iv) Ac_2O/DIPEA/DMF, rt, 15 min; h) TFA/EDT/TIPs/water (95:2:2:1, *v/v/v/v*), rt, 2 h; i) 50 % TFA/DMSO, rt, 20 min; j) i) 20 % piperidine/DMF, rt, 15 min twice; ii) Fmoc-AA-OH, HCTU, DIPEA, DMF, rt, 30 min; iii) 20 % piperidine/DMF, rt, 15 min twice; iv) **14**, HATU, HOAt, DIPEA, DMF, rt, 2 h; k) $Pd(PPh_3)_4$, $PhSiH_3$, DCM, rt, 3 h; ii) 20 % piperidine/DMF, rt, 10 min; iii) PyAOP, HOAt, NMM, NMP, rt, 12 h; iv) Ac_2O/DIPEA/DMF, rt, 15 min; l) TFA/EDT/TIPs/Water (95:2:2:1, *v/v/v/v*), rt, 2 h; The resin-bound peptides were protected on side chains at asterisk sites. The following protecting groups for amino acid side chains were used: tert-butyl (^{t}Bu; for Tyr and Glu), 2,2,4,6,7-pentamethyldihydrobenzo-furane-5-sulfonyl (pbf; for Arg), tert-butyloxycarbonyl (Boc; for Lys) and trityl (Trt; for Cys), 4-methoxybenzyl (Mob; for Sec).

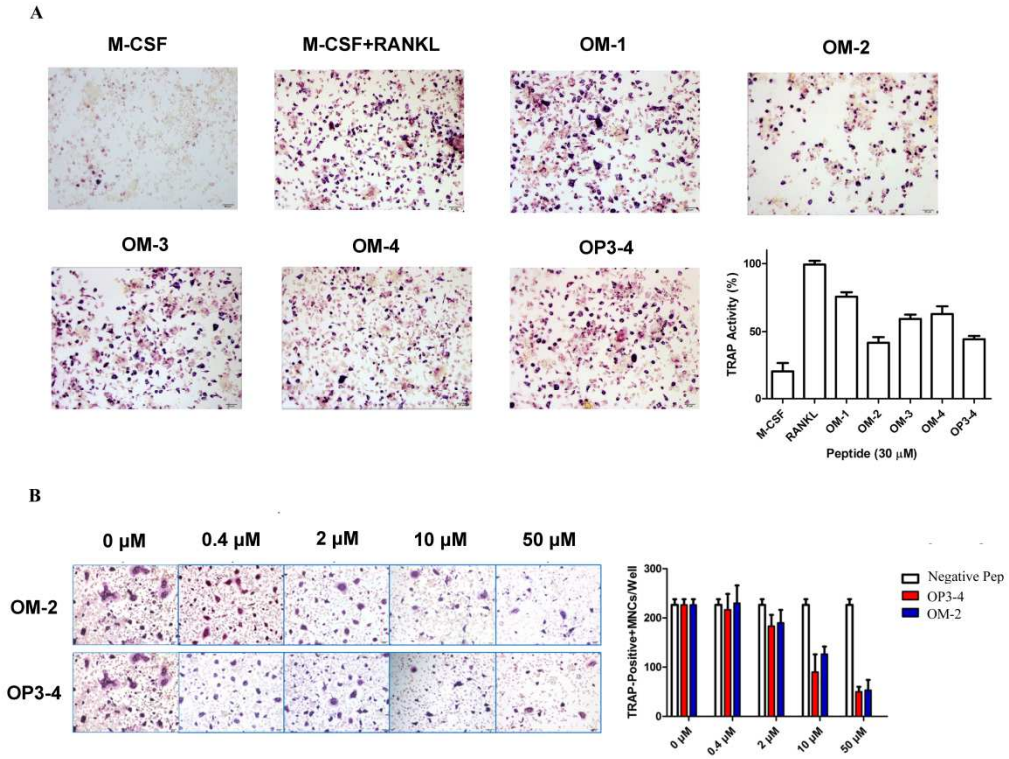

Figure 2. A) Inhibitory effects of OPG mimics on the sRANKL-induced osteoclast differentiation, estimated by the number of TRAP-positive multinucleated cells. B) Dose-dependent inhibition of OM-2 and OP3-4 on the sRANKL-induced osteoclast differentiation estimated by the number of TRAP-positive multinucleated cells. The results represent the mean value SEM of three independent experiments.

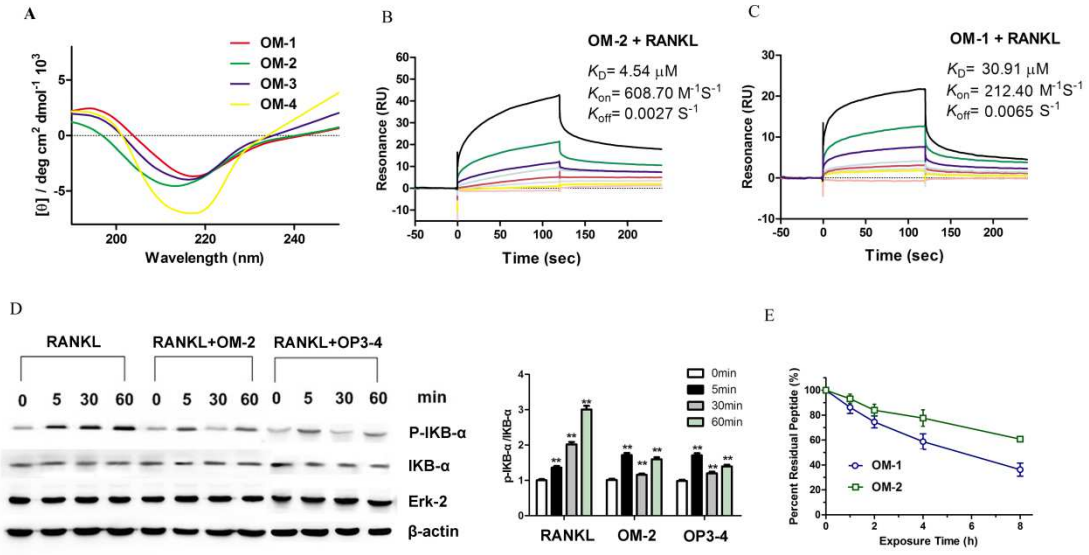

Figure 3. A) CD spectra of the peptides in 50% TFE aqueous solution at 20 °C. B) SPR binding studies of OM-2 to RANKL. C) SPR binding studies of OM-1 to RANKL. D) Effects of OM-2 and OP3-4 treatment on down-stream NF-κB signaling pathway by western blot. E) Proteolytic stability of OM-1 *vs.* OM-2 under α-chymotrypsin treatment. Data points are displayed as the mean value SEM of duplicate independent experiments. The percent residual peptide was monitored *via* HPLC.

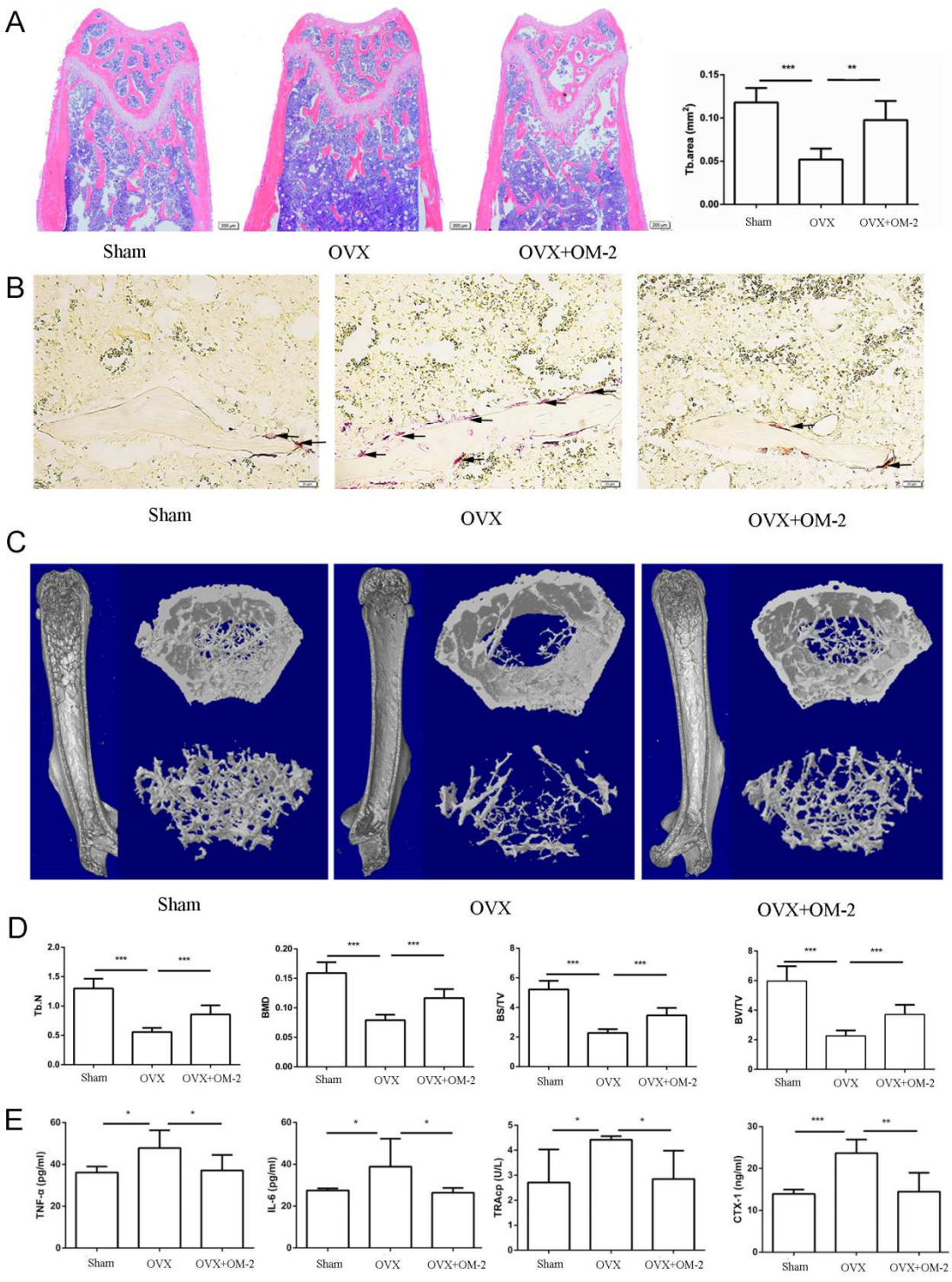

Figure 4. OM-2 reduces ovariectomy-induced bone loss *in vivo*. A) Representative H&E staining of distal femoral sections and quantification of trabecular area. B) Representative TRAP-stained histologic distal femur sections from sham, OVX and OVX + OM-2 group. C) Micro CT analysis of the distal femur from sham, OVX, and OVX + OM-2 group. D) Calculations of trabecular number (Tb.N), bone surface area/ tissue volume (BS/TV), bone volume / tissue volume (BV/TV) and bone mineral density (BMD). E) Serum IL-6, TNF-α, TRAcp 5B and CTX-1 were examined (*P < 0.05, **P < 0.01, ***P < 0.001).

Highlights

1. We disclose the successful development of a novel glycopeptide, which exhibited potent binding affinity with RANKL and resistance to degradation by protease enzymes.

2. This novel glycopeptide is suggested as a therapeutic candidate for postmenopausal osteoporosis (PMOP) and osteoclastogenesis-related diseases like rheumatoid arthritis (RA).